Analysis and generation of chaos using compositely connected coupled memristors

Ciyan Zheng, Herbert H. C. Iu, Tyrone Fernando, Dongsheng Yu, Hengdao Guo, and Jason K. Eshraghian

Citation: Chaos **28**, 063115 (2018); doi: 10.1063/1.5023142
View online: https://doi.org/10.1063/1.5023142
View Table of Contents: http://aip.scitation.org/toc/cha/28/6
Published by the American Institute of Physics

Analysis and generation of chaos using compositely connected coupled memristors

Ciyan Zheng,[1,a)] Herbert H. C. Iu,[1,a)] Tyrone Fernando,[1] Dongsheng Yu,[2] Hengdao Guo,[1,a)] and Jason K. Eshraghian[1]
[1]*The School of Electrical, Electronic and Computer Engineering, the University of Western Australia, Crawley, Perth, WA 6009, Australia*
[2]*The School of Electrical and Power Engineering, China University of Mining and Technology, Xuzhou 221116, China*

(Received 22 January 2018; accepted 25 May 2018; published online 15 June 2018)

In large-scale high-density integrated circuits, memristors in close proximity to one another both influence, and are influenced by, the behavior of nearby memristors. However, the previous analyses of memristors-based circuit applications have seldom considered the possibility of coupling effects between memristors which invariably influences the response of all memristors, thus rendering much previous research as incomplete. In this paper, the circuit dynamics of memristive Chua's circuits are systematically analyzed based on a pair of compositely connected flux-controlled memristors characterized by cubic nonlinearity as a typical example. A theoretical analysis is undertaken and verified via MATLAB. While tuning the coupling strength, variations in circuit dynamics are characterized by phase portraits, bifurcation diagrams, and Lyapunov exponents. A new floating memristor emulator with coupling ports, described by cubic nonlinearity, is designed using off-the-shelf circuit devices and is shown to be successfully used in building chaotic circuits in hardware experiments, verifying theoretical results in simulations. This paper provides a new way through which memristors-based circuit dynamics can be influenced by tuning the coupling strength between memristors without changing other circuit parameters. It is further highlighted that when designing future memristors-based circuits, the coupling action between memristors should be considered if necessary and compensated when causing undesired circuit responses. *Published by AIP Publishing.* https://doi.org/10.1063/1.5023142

The memristor (MR) is the fourth basic circuit element. In recent years, many large-scale high-density integrated circuit applications based on memristors have been developed due to the nanoscale size advantage and memory retention capabilities of memristors. When densely placed in circuits, behaviors of multiple memristors will be influenced by the interaction between them, which may cause undesired or unexpected circuit dynamics. In this paper, we investigate how the coupling behavior between memristors will influence chaotic dynamical behaviors of memristors-based Chua's circuit as an example to illustrate the importance of building a more accurate memristor model considering the memristive coupling action.

I. INTRODUCTION

Since its conceptualization in 1971 by Leon Chua[1] and its physical realization in 2008 by the Hewlett Packard labs,[2] the memristor (MR) has become an increasingly important candidate for building large-scale high-density integrated circuits due to its nanoscale size advantage and memory retention capabilities. Numerous studies have embedded these advantages into MRs-based applications, such as neural network systems,[3–6] memcomputing architectures,[7–9] memristive crossbar arrays,[10,11] and so forth. Once realized in the industry, these applications require MRs to operate in conjunction with one another in close physical proximity. Whether MR will exhibit unique characteristics when interacting with other MRs in tightly spaced configurations as compared with the case where only one MR is used in the circuit is worthy of research attention.

In the past, due to the fact that MRs are not commercially available, tremendous effort has been put into dissecting the inherent characteristics of MRs on the basis of simulation models.[12–14] Besides, practical MR emulators are also proposed for experimental investigations by making use of off-the-shelf electronic circuit devices.[14,15] Solid-state MRs were commercialized by Knowm and Bio-inspired Technologies in 2015, but unlike resistors, they suffer from severe limitations in that they are expensive and can only operate under very strict conditions according to their datasheets. Therefore, building MR emulators for disclosing dynamic behaviors of MRs and developing potential MRs-based applications are still necessary.

Dynamic behaviors of multiple connected MRs are far richer than those of single MR because MRs are sensitive to their polarity configuration. Unlike the other three fundamental circuit devices (namely, the resistor, capacitor, and inductor), a MR exhibits different dynamics when the polarity of a MR device is changed, whether in a network or as a standalone MR. Based on MR mathematical models or

a)Authors to whom correspondence should be addressed: ciyan.zheng@research.uwa.edu.au, herbert@ee.uwa.edu.au, and hengdao.guo@research.uwa.edu.au.

emulating methods, multiple interconnected MRs have been examined across a large body of work: the research in Refs. 15–17 explored the comprehensive behaviors of MRs connected in series and parallel, and the work in Refs. 18–20 discovered new applications based on MRs by specifying certain polarity combinations.

However, when developing MRs-based circuit models, inaccuracies often exist. For example, when calculating the internal state of MRs, one problem with the use of certain types of MRs is the often overlooked thermodynamic constraints and inconsistency with electrochemical equilibrium.[21] The initial MR state conditions are susceptible to self-diffusion and may shift to absolute equilibrium states as determined by the device material. Besides, when developing multiple MRs-based circuits, the interaction between is also an important factor due to the physical inaccuracy of present MR models. Solid-state MRs might not be guaranteed to behave as modeled, thus resulting in unexpected performance from a circuit while developing MRs-based applications.

Recent work has highlighted that in addition to series and parallel connections between MRs, "coupling" is defined as a third unique relation between MRs via their state variables,[22] with two special examples of thermal and mechanical coupled memristive and memcapacitive systems investigated by means of simulation. Researchers then built mathematical models to characterize the coupling action via state variables in the early research stage. The work in Ref. 23 conducted simulation-based analysis on the coupling action between MRs and the work in Refs. 24–27 made use of MR hardware emulators to mimic the coupling action through connecting emulators together by using circuit wires or use the inductive coupling of the constitutive inductors in MR emulators to realize wireless coupling between MRs, ascertaining how one MR can affect the circuit dynamics of another MR. These models theoretically describe how the interaction between MRs can influence the memristive behaviors of another MR, and the results provided in these papers were shown to disclose the inherent coupling characteristics of MRs beforehand, facilitating the future research on the coupling behavior between solid-state MRs. When modeling the coupling process between MRs, state variables are often selected as the coupling term and the reason is described as follows. As shown in Ref. 1, MRs can be categorized into flux-controlled or charge-controlled ones, with flux and charge as their state variables, and a MR model is characterized based on fundamental constitutive relationships between state variables. If we use equations to correlate state variables of two MRs, a relation of coupling can be defined for the two memristive systems. This coupling relation shows that state variables of each MR can influence or be influenced by the state variables of the other, and the values of memristance and memristive behaviors for each MR are influenced correspondingly.

It is known that memory elements have information storage functions, similar as capacitors and inductors with the ability to store positive energy and it is also well known that there exist coupling effects between densely packed inductors and very adjacent capacitors in electric circuits via magnetic or electric fields. Besides, it has been pointed out that the integrated circuit comprising multiple hardware TiO_2 MRs has mutual capacitances and inductances between MRs, and the mutual parameters are influenced by the size and position of each MR cell.[28] Torrenzan *et al*. put forward a sub-nanosecond switching of a metal-oxide-metal MR considering the parasitic capacitance, and at the same time studied how to minimize its parasitic effects on the switching behaviors of MR.[29] Many researchers have studied how to integrate these parasitic parameters in the circuit modeling of MRs and how these parameters can affect the characteristics of MRs.[30,31] Based on these facts, a reasonable and generalized assumption throughout this paper is made according to characteristics of the parasitic capacitive coupling and the inductive coupling, that is, the coupling strength between solid-state MRs is related to the position of each MR cell when MRs are densely placed.

Due to the intrinsic nonlinearity of the MR, it plays an important role in building chaotic or hyperchaotic circuits. The development of various MR-based chaotic or hyperchaotic circuits shows the potential application of MRs in secure encryption, image encryption, and weak signal detection. Examples of cases where single MRs were used to build chaotic circuits are shown[32–35] and examples where multiple MRs were used compositely to build chaotic circuits are examined.[36–39] Furthermore, MR coupling will unavoidably introduce additional physical dependencies that will be shown to be capable of affecting chaotic dynamics within a circuit composed of two or more MRs; thus, we should take this possible influencing factors into consideration. For example, if the coupling strength between a pair of MRs is specified to certain values, then chaos in MRs-based circuits can still be generated in situations where it would otherwise not be possible. Coupling may result in shifts in the dynamical responses of MR-based circuits, and in the utilitarian view, the dynamical behaviors of circuits can be tuned according to different values of the coupling strength between MRs.

However, very little research implements the interaction between MRs to chaotic circuit applications. One paper has explored the spontaneous synchronization of two Chua's circuits based on coupled MRs.[25] Nevertheless, there are no experimental results given and the MR emulator proposed in this paper is restricted by having one terminal connected to the ground, which severely limits emulation of compositely connected MRs with other circuit components in series. Other present knowledgebase in the application of MRs in chaotic circuits utilizing the term "coupling" is to utilize the MR as an interconnecting device to couple two other separate circuits, and hence labeled as "coupled,"[18,40–43] but not the same term as the "coupling" in this paper.

In addition to MRs-based chaotic circuits, the coupling effect between MRs should also be considered in other MRs-based applications, with undesired circuit responses mitigated if necessary. However, many other MRs-based applications have been developed and no matter in mathematical modeling, simulations, or in experimentation, the interaction between MRs is rarely accounted for.[3–11] As a result, when analyzing memristive circuits, a large proportion of present

research does not fully characterize the circuit dynamical responses; the analyses and models used are incomplete and potentially inaccurate.

This work serves to extend the fundamental theory of MRs-based circuits by using coupled MRs connected in different polarity configurations to structure chaotic circuits. More importantly, in view of the lack of practical circuit applications for the coupling action between MRs, the circuits in this paper are used as typical examples to shed light on how to analyse the variation of system dynamics as a function of the coupling strength between MRs. We should integrate the interaction between MRs into the process of memristive circuit designing in order to see how the coupling will affect the circuit dynamical responses rather than as an afterthought or remedy to compensate for some undesired or unexpected performance from a memristive circuit.

This paper follows a systematic method in analyzing the system dynamics of compositely connected MRs-based chaotic circuits. Section II is devoted to developing MR models with cubic nonlinearities based on the fundamental constitutive relationships between charge and flux. In Sec. III, the models presented are used to simulate the circuit dynamics of the chaotic circuit based on coupled MRs in MATLAB. We investigate the complex dynamics in terms of phase portraits, bifurcation diagrams, and Lyapunov exponent plots through varying the coupling strength between MRs. Section IV presents a novel emulator based on mathematical models for MR presented in Sec. II by using off-the-shelf circuit components and features coupling ports in order to mimic the coupling action between multiple MR emulators. Section V synthesizes the MR emulator in PSpice and confirms the feasibility to couple a pair of MRs together. Section VI performs experimental verification of the simulation results and elaborates upon how chaotic circuits based on MRs can be built and experimentally tested with regard to their dynamic behaviors in breadboard circuits. Contemplation of extension of this work is provided in the conclusion.

To summarize, the four primary aims of this paper are (1) to put forward a novel practical flux-controlled floating MR emulator with cubic nonlinearity. The emulator can be coupled with other MR emulators and all together play an important role in the generation of chaos in chaotic circuits; (2) to show the significance of taking the interaction, especially the coupling action between multiple MRs into consideration while designing memristive chaotic circuits. Investigation of how the coupling behavior and interconnections between MRs can bring about new circuit dynamics, which may be taken advantage of to develop other new circuits, or otherwise to mitigate their effects in presently existing circuits; (3) to provide a new possible method to tune chaotic behaviors in MRs-based chaos circuits via tuning the coupling strength, and (4) to provide a new memristive application in the chaotic circuits range based on coupled MRs.

II. COUPLED MRS

The MR models are developed based on the fundamental constitutive relationships between state variables charge and flux and can be classified as either charge-controlled or flux-controlled as defined in Ref. 1. Figure 1(a) shows the symbol of the MR with the polarity indicated by a black bar at one end. The relationship between the current and the voltage of a flux-controlled MR can be described as

$$i(t) = W(\varphi)v(t), \tag{1}$$

where t is the time, $v(t)$ denotes the voltage across the MR, φ denotes the flux, or otherwise the time integral of the voltage $v(t)$. Memductance W is defined as the reciprocal of the value of memristance and is expressed as

$$W(\varphi) = \frac{dq(\varphi)}{d\varphi}, \tag{2}$$

which reflects how W is the slope of the $q-\varphi$ curve, where q denotes the charge, or otherwise the time integral of the current $i(t)$.

A variety of MR models with different mathematical descriptions have been widely used in chaotic circuits for producing chaotic signals. For example, piecewise linearity,[44–46] piecewise quadratic,[46] cubic nonlinearity,[47–50] quintic nonlinearity,[51] and high-order nonlinear MRs.[52] In this work, we adopt such a nonlinear cubic relationship for the $q-\varphi$ function of the flux-controlled cubic memductance

$$q(\varphi) = \frac{1}{3}\alpha\varphi^3 + \beta\varphi. \tag{3}$$

The memductance W can thus be given by

$$W(\varphi) = \alpha\varphi^2 + \beta, \tag{4}$$

where α denotes the variation rate of the memductance and β represents the initial memductance value.

As explained in the Introduction, the coupling action enables one MR to influence or be influenced by the state-variable(s) of another MR.[22,24] Due to the fact that the flux and the charge are two intrinsic state variables related to memductance, MRs can thus be considered as either coupled by the flux or coupled by the charge. Figure 1(b) graphically represents the coupling action between multiple MRs in high-density memristive applications. This illustration can be extended to as many MRs beyond the four that are depicted. Voltage v_{A1B1} denotes the voltage between the two terminals of MR1; v_{A2B2} denotes the voltage between the two terminals of MR2; v_{AnBn} denotes the voltage between the two terminals of MR$_n$. Expressions of the memductance functions $W_1(\varphi)$, $W_2(\varphi)$ to $W_n(\varphi)$ with cubic nonlinearities of flux-controlled coupled MRs can be described by the following set of equations:

$$W_1(\varphi) = \alpha_1\varphi_{A1B1}^2 + \beta_1 + f_{12}(\varphi_{A2B2}) + f_{13}(\varphi_{A3B3}) + \cdots + f_{1n}(\varphi_{AnBn}), \tag{5a}$$

$$W_2(\varphi) = \alpha_2\varphi_{A2B2}^2 + \beta_2 + f_{21}(\varphi_{A1B1}) + f_{23}(\varphi_{A3B3}) + \cdots + f_{2n}(\varphi_{AnBn}), \tag{5b}$$

$$W_n(\varphi) = \alpha_n\varphi_{AnBn}^2 + \beta_n + f_{n1}(\varphi_{A1B1}) + f_{n2}(\varphi_{A2B2}) + \cdots + f_{n(n-1)}(\varphi_{An-1Bn-1}), \tag{5c}$$

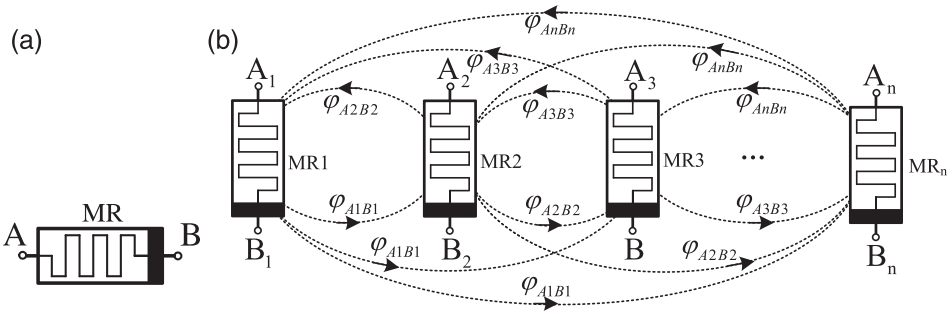

FIG. 1. (a) Symbol of the memristor MR and (b) multiple coupled MRs from MR1 to MR_n.

where the flux represented by φ_{AnBn} denotes the time integral of the voltage v_{AnBn} across MR_n, and the function $f_{xy}(\varphi)$ represents the coupling action from MRy to MRx and can be defined according to the coupling strength between nanoscale MRs in real life. To simplify the circuit analysis, only two coupled MRs, MR1 and MR2, are adopted for demonstration. For simplicity of further realizing the mathematical description of MR in simulation and hardware experiments, the functions $f_{12}(\varphi_{A1B1})$ and $f_{21}(\varphi_{A1B1})$ are configured using simple quadratic functions for simplicity in circuit implementation

$$f_{12}(\varphi_{A2B2}) = \kappa_1 \varphi_{A2B2}^2, \tag{6a}$$

$$f_{21}(\varphi_{A1B1}) = \kappa_2 \varphi_{A1B1}^2. \tag{6b}$$

Consequently, by substituting (6a) and (6b) into (5a)–(5c), memductance of a pair of MRs can be ascertained by

$$W_1(\varphi_{A1B1}, \varphi_{A2B2}) = \alpha_1 \varphi_{A1B1}^2 + \beta_1 + \kappa_1 \varphi_{A2B2}^2, \tag{7a}$$

$$W_2(\varphi_{A2B2}, \varphi_{A1B1}) = \alpha_2 \varphi_{A2B2}^2 + \beta_2 + \kappa_2 \varphi_{A1B1}^2, \tag{7b}$$

where the coupling strengths between these two MRs are reflected by coupling coefficients κ_1 and κ_2. Hence, these two MRs can be easily configured into tightly or loosely coupled by adjusting coefficients κ_1 and κ_2. The research presented in Secs. III–VI focuses on a single pair of MRs coupled together in varying modes of connections. The work presented can be extended to apply to coupling between n MRs, as shown in Fig. 1(b).

III. MEMRISTIVE CHAOTIC CIRCUITS AND SIMULATION RESULTS

In this section, memristive chaotic circuits based on coupled MRs are analyzed. Two MRs are connected in series or parallel and are mutually coupled through the flux. The two MRs, MR1 and MR2, are used to replace Chua's diode in Chua's circuit.

A. Memristive Chua's circuit based on serially connected MRs with identical polarities

Here, in Subsections III A and III B, v_{11} is the voltage across the capacitor C_1; v_{21} is the voltage across the capacitor C_2; i_L is the current flowing through the inductor L_1; voltages v_{A1B1}, v_{A2B2} are voltages across MR1 and MR2; and voltages v_{01} and v_{02} serve as the reference directions for the voltage across MRs, as shown in Fig. 2. Flux values φ_{A1B1}, φ_{A2B2}, φ_1, φ_2 represent the time integral of voltages v_{A1B1}, v_{A2B2}, v_{01}, and v_{02}, respectively, and φ_{11} represents the time integral of voltage v_{11}. W_1 and W_2 represent the memductance of MR1 and MR2, respectively. W_{11} represents the total memductance for connected MRs.

By connecting the terminal B1 to A2 of two MRs in Fig. 1(b), two coupled MRs are serially connected with identical polarity configurations. The coupled MRs are applied to Chua's circuit, as shown in Fig. 2. By applying Kirchhoff's Voltage Law (KVL), the voltage and current across A1 and B2 can be calculated using

$$v_{01}(t) = v_{A1B1}(t), \quad v_{02}(t) = v_{A2B2}(t), \tag{8a}$$

$$v_{11}(t) = v_{01}(t) + v_{02}(t), \tag{8b}$$

$$i(t) = v_{01}(t) W_1(\varphi_1, \varphi_2) = v_{02}(t) W_2(\varphi_2, \varphi_2). \tag{8c}$$

Integration of both sides of (8a) leads to (9a), and likewise (8b) leads to (9b)

$$\varphi_1 = \varphi_{A1B1}, \quad \varphi_2 = \varphi_{A2B2}, \tag{9a}$$

$$\varphi_{11}(t) = \varphi_1(t) + \varphi_2(t). \tag{9b}$$

Substitution of (9a) into (7a) and (7b) produces the following result:

$$W_1(\varphi_1, \varphi_2) = \alpha_1 \varphi_1^2 + \beta_1 + \kappa_1 \varphi_2^2, \tag{10a}$$

$$W_2(\varphi_2, \varphi_1) = \alpha_2 \varphi_2^2 + \beta_2 + \kappa_2 \varphi_1^2, \tag{10b}$$

and the total memductance $W_{11}(\varphi_1, \varphi_2)$ of MRs serially connected together can be expressed as

$$W_{11} = \frac{W_1 W_2}{W_1 + W_2} = \frac{(\alpha_1 \varphi_1^2 + \beta_1 + \kappa_1 \varphi_2^2)(\alpha_2 \varphi_2^2 + \beta_2 + \kappa_2 \varphi_1^2)}{\alpha_1 \varphi_1^2 + \alpha_2 \varphi_2^2 + \beta_1 + \beta_2 + \kappa_1 \varphi_2^2 + \kappa_2 \varphi_1^2}. \tag{11}$$

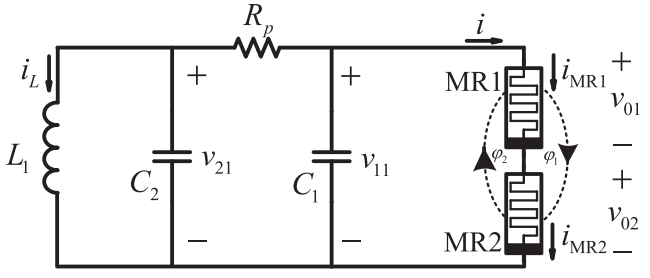

FIG. 2. Memristive Chua's circuit based on coupled MRs connected in series with identical polarities.

Substituting (9b), (10a), and (10b) into (8c) gives the following equations:

$$\begin{cases} \dfrac{d\varphi_1}{dt}\left(\alpha_1\varphi_1^2+\beta_1+\kappa_1\varphi_2^2\right) \\ \quad=\left(\dfrac{d\varphi_{11}}{dt}-\dfrac{d\varphi_1}{dt}\right)\times\left(\alpha_2\varphi_2^2+\beta_2+\kappa_2\varphi_1^2\right), \\ \left(\dfrac{d\varphi_{11}}{dt}-\dfrac{d\varphi_2}{dt}\right)\left(\alpha_1\varphi_1^2+\beta_1+\kappa_1\varphi_2^2\right) \\ \quad=\dfrac{d\varphi_2}{dt}\times\left(\alpha_2\varphi_2^2+\beta_2+\kappa_2\varphi_1^2\right). \end{cases} \tag{12}$$

Thus, the derivative of φ_1 and φ_2 are expressed as

$$\begin{cases} \dfrac{d\varphi_1}{dt}=\dfrac{v_{11}(t)(\alpha_2\varphi_2^2+\beta_2+\kappa_2\varphi_1^2)}{\alpha_1\varphi_1^2+\alpha_2\varphi_2^2+\beta_1+\beta_2+\kappa_1\varphi_2^2+\kappa_2\varphi_1^2}, \\ \dfrac{d\varphi_2}{dt}=\dfrac{v_{11}(t)(\alpha_1\varphi_1^2+\beta_1+\kappa_1\varphi_2^2)}{\alpha_1\varphi_1^2+\alpha_2\varphi_2^2+\beta_1+\beta_2+\kappa_1\varphi_2^2+\kappa_2\varphi_1^2}. \end{cases} \tag{13}$$

Since expressions of φ_1 and φ_2 in (12) can be hardly resolved based on analytical methods, expressions of the derivative of φ_1 and φ_2 are directly used in the set of differential equations. Based on the circuit theory, the following set of equations of this high order system can be depicted by

$$\begin{cases} \dfrac{d\varphi_1(t)}{dt}=\dfrac{v_{11}(t)(\alpha_2\varphi_2^2+\beta_2+\kappa_2\varphi_1^2)}{\alpha_1\varphi_1^2+\alpha_2\varphi_2^2+\beta_1+\beta_2+\kappa_1\varphi_2^2+\kappa_2\varphi_1^2}, \\ \dfrac{d\varphi_2(t)}{dt}=\dfrac{v_{11}(t)(\alpha_1\varphi_1^2+\beta_1+\kappa_1\varphi_2^2)}{\alpha_1\varphi_1^2+\alpha_2\varphi_2^2+\beta_1+\beta_2+\kappa_1\varphi_2^2+\kappa_2\varphi_1^2}, \\ \dfrac{dv_{11}(t)}{dt}=\dfrac{1}{C_1}\left(\dfrac{v_{21}(t)-v_{11}(t)}{R_p}-v_{11}(t)W_{11}\right), \\ \dfrac{dv_{21}(t)}{dt}=\dfrac{1}{C_2}\left(\dfrac{v_{11}(t)-v_{21}(t)}{R_p}-i_L(t)\right), \\ \dfrac{di_L(t)}{dt}=\dfrac{v_{21}(t)}{L_1}. \end{cases} \tag{14}$$

The system of equations presented in (14) are solved in MATLAB, which present a mathematical model of the response from memristive Chua's circuit when two serially connected MRs are coupled with identical polarities. Phase portraits, Lyapunov exponents, and bifurcation diagrams are used to investigate the basic dynamics of the modified memristive Chua's circuit based on coupled MRs. The initial values for the system variables are set as $(\varphi_1,\ \varphi_2,\ v_{11},\ v_{21},\ i_L)=(0,\ 0,\ 0.11,\ 0.11,\ 0)$. Simulation parameters for the case where MRs are connected in series are $L_1=13.6$ mH, $R_p=1700\ \Omega$, $C_1=13$ nF, $C_2=268$ nF, $\alpha_1=\alpha_2=262$ mS/Wb^2, $\beta_1=\beta_2=1.43\times10^{-3}$ mS, and $\kappa_2=61$ mS/Wb^2.

By adjusting the coupling strength κ_1, which is set as the bifurcation parameter, dynamical behaviors of this chaotic circuit are able to simultaneously change. When the value of κ_1 increases, the phase plane plot changes from period-1 limit cycle to the chaotic attractor. When $\kappa_1=38$ mS/Wb^2, the phase plane plot is in a period-1 state and when $\kappa_1=7600$ mS/Wb^2, it is in a chaotic state. The results of phase portraits for $v_{11}-v_{21}$, φ_1-v_{11}, φ_1-v_{21} are shown in Fig. 3.

Figure 4 shows corresponding time-domain waveforms of variables v_{11} and v_{21} in periodic and chaotic states.

The coupling strength κ_1 between two MRs acts as a varying parameter set between the values [0, 1×10^4 mS/Wb^2]. Figures 5(a) and 5(b) present the bifurcation diagram of the state variable v_{11} and the corresponding Lyapunov exponent spectrum of the memristive Chua's circuit based on coupled MRs connected in series with identical polarities. The legend of Fig. 5(b) displays LE1 to LE5, denoting the values of five Lyapunov exponents, respectively. Note that the presence of chaos is indicated when one of the Lyapunov exponents is positive and the sum of the exponents is negative.[49] If the maximum Lyapunov exponent of the system of equations in (14) is larger than zero, the system is in a chaotic state, and if the maximum Lyapunov exponent is equal to zero, the system is in a periodic state. When the coupling strength κ_1 increases, the dynamics of the proposed circuit commences with exhibiting periodic behaviors, and then enters into chaotic behaviors via a forward periodic-doubling bifurcation route. Correspondingly, the maximum Lyapunov exponents have a transition from zero values to positive values. In the chaotic region, there exist one periodic window [4.62×10^3 mS/Wb^2 and 6.44×10^3 mS/Wb^2], in which the maximum Lyapunov exponent is equal to zero. The bifurcation diagram coincides well with the Lyapunov exponents' spectrum.

Thus, in this case, where Chua's circuit is built based on coupled MRs connected in series with identical polarities under a specific parameter configuration, when the coupling

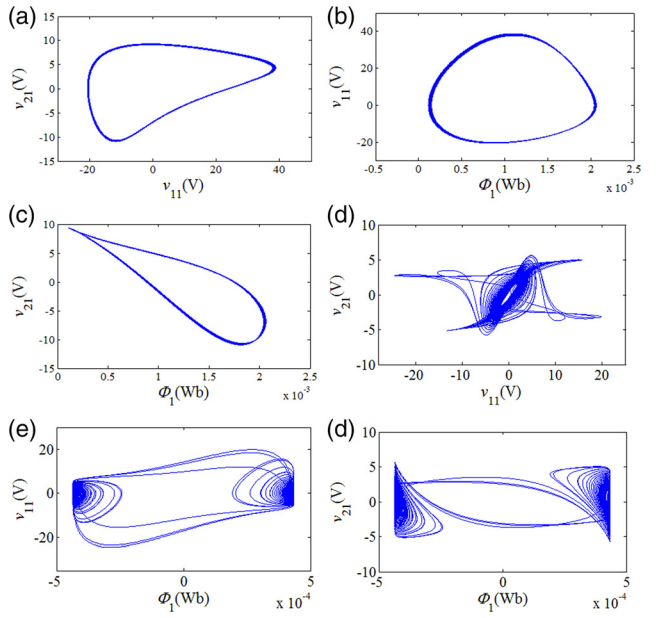

FIG. 3. Projections of periodic orbits at $\kappa_1=38$ mS/Wb^2 on the (a) $v_{11}-v_{21}$ plane; (b) φ_1-v_{11} plane; (c) φ_1-v_{21} plane, as well as projections of typical chaotic attractor at $\kappa_1=7600$ mS/Wb^2 on the (d) $v_{11}-v_{21}$ plane; (e) φ_1-v_{11} plane; and (f) φ_1-v_{21} plane.

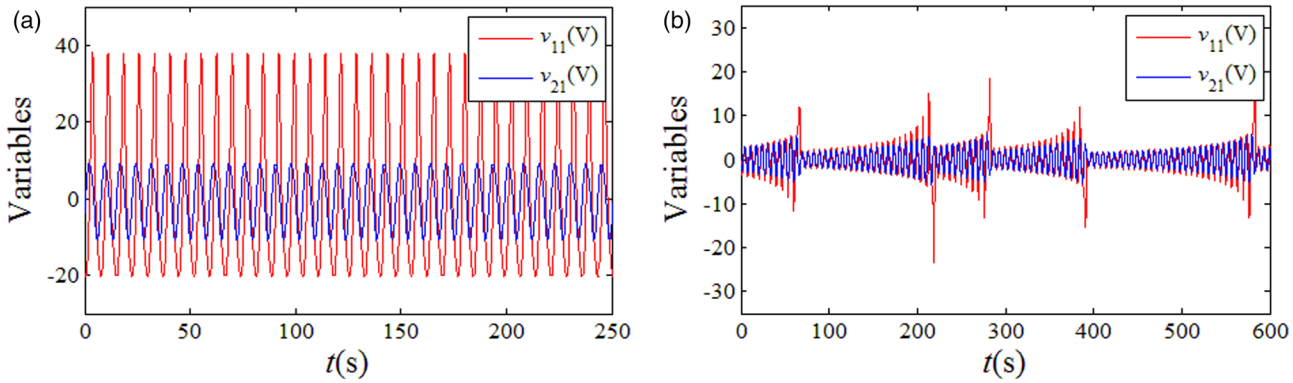

FIG. 4. Time-domain waveforms in the time interval [0 s, 250 s] when (a) the system is periodic at $\kappa_1 = 38$ mS/Wb^2 and (b) the system is chaotic at $\kappa_1 = 7600$ mS/Wb^2.

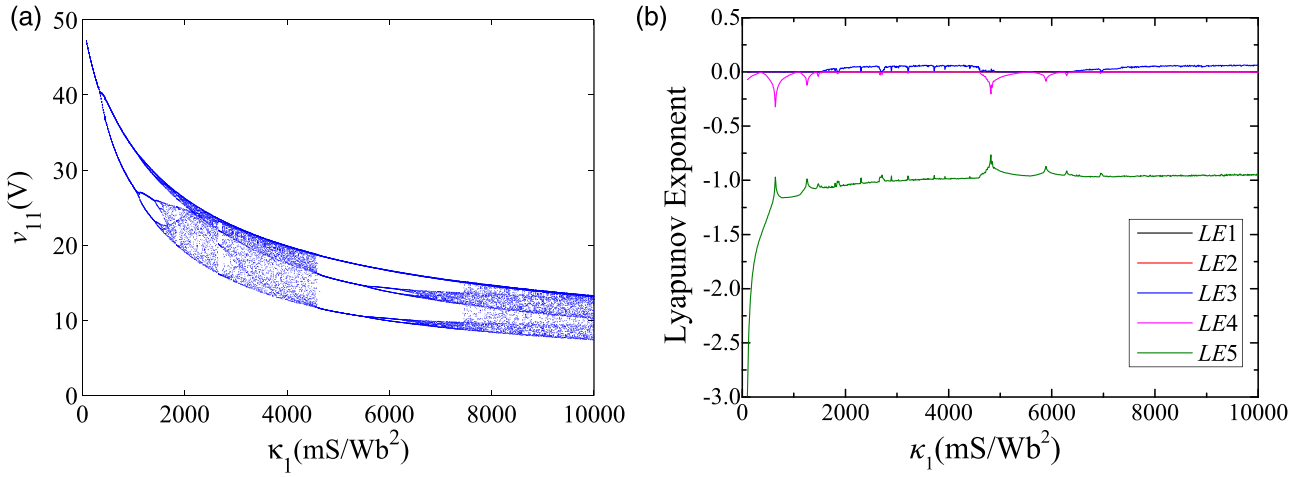

FIG. 5. Dynamical behaviors of the memristive circuit with κ_1 increasing: (a) bifurcation diagram with respect to κ_1 and (b) Lyapunov exponent spectrum with respect to κ_1.

strength κ_1 increases, the transition in circuit dynamics from one cycle to chaos is observed.

B. Memristive Chua's circuit based on serially connected MRs with opposite polarities

When MRs are connected in series with opposite polarities, the relationship between $\varphi_{A1B1}, \varphi_1, \varphi_{A2B2}, \varphi_2$ can be expressed as

$$\varphi_1 = \varphi_{A1B1}, \varphi_2 = -\varphi_{A2B2}. \tag{15}$$

According to (9a), (10a), (10a), (12), and (15), it can be found that when MRs are connected in series with opposite polarities, the set of differential equations are identical to the equations in the scenario where MRs are connected in series with identical polarities. This is because the quadratic functions for $f_{12}(\varphi_{A2B2})$ and $f_{21}(\varphi_{A1B1})$ defined in (6a) and (6a) eliminate the effects of the polarity switching of fluxes φ_{A1B1} and φ_{A2B2}. Thus, the case where MRs are connected in series with opposite polarities can be understood by referring to Subsection III A where they are connected with identical polarities, and need not be further explained.

C. Memristive Chua's circuit based on parallel connected MRs with identical polarities

In Subsections III C and III D, v_{11} is the voltage across the capacitor C_1; v_{21} is the voltage across the capacitor C_2; i_L is the current flowing through the inductor L_1; voltages v_{A1B1}, v_{A2B2} are voltages across MR1 and MR2; and the voltage v_{11} serves as the reference direction for the voltage across MRs, as shown in Fig. 6. Flux values $\varphi_{11}, \varphi_1, \varphi_2$ represent the time integral of voltages v_{11}, v_{01}, and v_{02}, respectively. As $v_{11} = v_{A1B1} = v_{A2B2} = v_{01} = v_{02}, \varphi_{11}$ is used to represent the value of fluxes of φ_{A1B1} and φ_{A2B2}. W_{11}

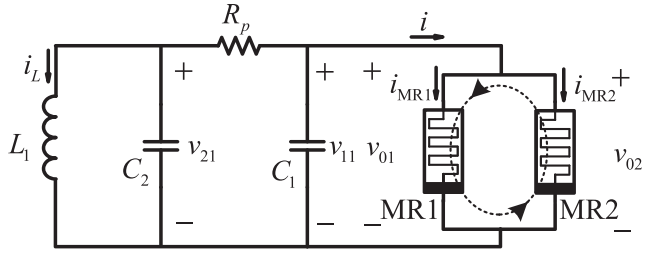

FIG. 6. Memristive Chua's circuit based on coupled MRs connected in parallel with identical polarities.

represents the total memductance for connected MRs. By reference to two MRs in Fig. 1, connecting terminals A1 to A2 and B1 to B2, we realize two MRs connected in parallel with identical polarities. The coupled MRs are implemented into Chua's circuit, as shown in Fig. 6. The current passing through terminals A1 and B2 as well as the flux φ_{11} can be represented using the following equations:

$$i(t) = i_1(t) + i_2(t), \tag{16}$$

$$\varphi_{11}(t) = \varphi_1(t) = \varphi_2(t). \tag{17}$$

According to Kirchhoff's Current Law (KCL), the following equation holds:

$$\begin{aligned} i(t) = {} & v_{01}(t)(\alpha_1\varphi_1^2 + \beta_1 + \kappa_1\varphi_2^2) \\ & + v_{02}(t)(\alpha_2\varphi_2^2 + \beta_2 + \kappa_2\varphi_1^2). \end{aligned} \tag{18}$$

By integrating both sides of (18), the following equation is realized:

$$q = \frac{1}{3}(\alpha_1 + \alpha_2 + \kappa_1 + \kappa_2)\varphi_{11}^3 + (\beta_1 + \beta_2)\varphi_{11}. \tag{19}$$

Using (4) and (19), the total memductance $W_{11}(\varphi_{11})$ of dual coupled MRs connected in parallel with identical polarities can be calculated as

$$W_{11}(\varphi_{11}) = \frac{dq(\varphi_{11})}{d\varphi_{11}} = (\alpha_1 + \alpha_2 + \kappa_1 + \kappa_2)\varphi_{11}^2 + \beta_1 + \beta_2. \tag{20}$$

Based on circuit theory, the system of equations of this high order system can be depicted by

$$\begin{cases} \dfrac{d\varphi_{11}(t)}{dt} = \dfrac{d\varphi_1(t)}{dt} = v_{11}(t), \\ \dfrac{dv_{11}(t)}{dt} = \dfrac{1}{C_1}\left(\dfrac{v_{21}(t) - v_{11}(t)}{R_p} - v_{11}(t)W_{11}\right), \\ \dfrac{dv_{21}(t)}{dt} = \dfrac{1}{C_2}\left(\dfrac{v_{11}(t) - v_{21}(t)}{R_p} - i_L(t)\right), \\ \dfrac{di_L(t)}{dt} = \dfrac{v_{21}(t)}{L_1}. \end{cases} \tag{21}$$

The system of equations presented in (21) are solved in MATLAB, which present a mathematical model of the response from memristive Chua's circuit when two parallel connected MRs are coupled with identical polarities. The initial values for the system variables are set as $(\varphi_{11}, v_{11}, v_{21}, i_L) = (0, 0.11, 0.11, 0)$.

Simulation parameters for the case where MRs are connected in parallel are $L_1 = 18$ mH, $R_p = 2000\ \Omega$, $C_1 = 6.8$ nF, $C_2 = 68$ nF, $\alpha_1 = \alpha_2 = \kappa_2 = 2.175 \times 10^{-5}$ mS/Wb^2, and $\beta_1 = \beta_2 = 2.7775 \times 10^{-4}$ mS. By adjusting the coupling strength κ_1, which is set as the bifurcation parameter, the dynamical behaviors of the chaotic circuit can be simultaneously influenced. When the value of κ_1 increases, the phase plane plot changes from the chaotic attractor to period-1 limit cycle. When $\kappa_1 = 10$ mS/Wb^2, the phase plane plot is in a chaotic state, and when $\kappa_1 = 400\text{S/Wb}^2$, the plot is in a period-1 state. The results of phase portraits for $v_{11} - v_{21}, \varphi_{11} - v_{11}, \varphi_{11} - v_{21}$ are shown in Fig. 7. Figure 8 shows the corresponding time-domain waveforms of variables v_{11} and v_{21} in chaotic and periodic states.

The coupling strength κ_1 between two MRs acts as a varying parameter and ranges between [0, 4.5×10^5 mS/Wb^2]. Figures 9(a) and 9(b) depict the bifurcation diagram of the state variable v_{11} and the corresponding Lyapunov exponent spectrum of Chua's circuit based on coupled MRs connected in parallel with identical polarities. The legend of Fig. 9(b) shows LE1 to LE4, denoting the values of four Lyapunov exponents, respectively. As the coupling parameter κ_1 increases, the dynamics of the proposed circuit initiates with chaotic behaviors and then settles down into periodic behaviors via an inverse periodic-doubling bifurcation route. In the region between [0, 4.5×10^5 mS/Wb^2], the system goes through two cycle windows in [5.45×10^4 mS/Wb^2, 7.89×10^4 mS/Wb^2] and [9.86×10^4 mS/Wb^2, 1.28×10^5 mS/Wb^2]. The bifurcation diagram coincides well with the Lyapunov exponents' spectrum.

Thus, in this case, where Chua's circuit is built based on coupled MRs connected in parallel with identical polarities under a specific parameter configuration, when the coupling strength κ_1 increases, the transition in circuit dynamics from chaos to one cycle is observed.

D. Memristive Chua's circuit based on parallel connected MRs with opposite polarities

Similar to Subsection III B, the case where MRs are connected in parallel with opposite polarities is not further explained because of $v_{11} = v_{A1B1} = v_{A2B2}$ and the equations defined in (6a) and (6b), the differential equations which model this scenario end up identical to the case in which MRs are connected in parallel with identical polarities.

Thus, in this section, we can conclude that the coupling strength between MRs has an impact on memristive circuit dynamical responses. It is also derived that in the simulation process of designing applications containing densely spaced MRs, it is necessary to consider the coupling action between MRs to accurately describe dynamical responses of MRs-based circuits and systems.

IV. EQUIVALENT CIRCUIT REALIZATION OF COUPLED MRs WITH CUBIC NONLINEARITY

Those existing MR emulators used in memristive chaotic circuits often have the restriction of one terminal requiring a connection to ground[20,46,50,51,53] or the difficulty to involve the coupling action between MRs into the modeling process. Therefore, designing a new floating MR emulator, with the capacity to be coupled as part of a chaotic circuit, is necessary in order to experimentally verify the theoretical analysis in Sec. III.

In this section, a floating MR emulator is first built up to mimic MRs that can be coupled together. The coupling behavior between MR emulators can be achieved by constitutive amplifiers, which are operating as analog adders.

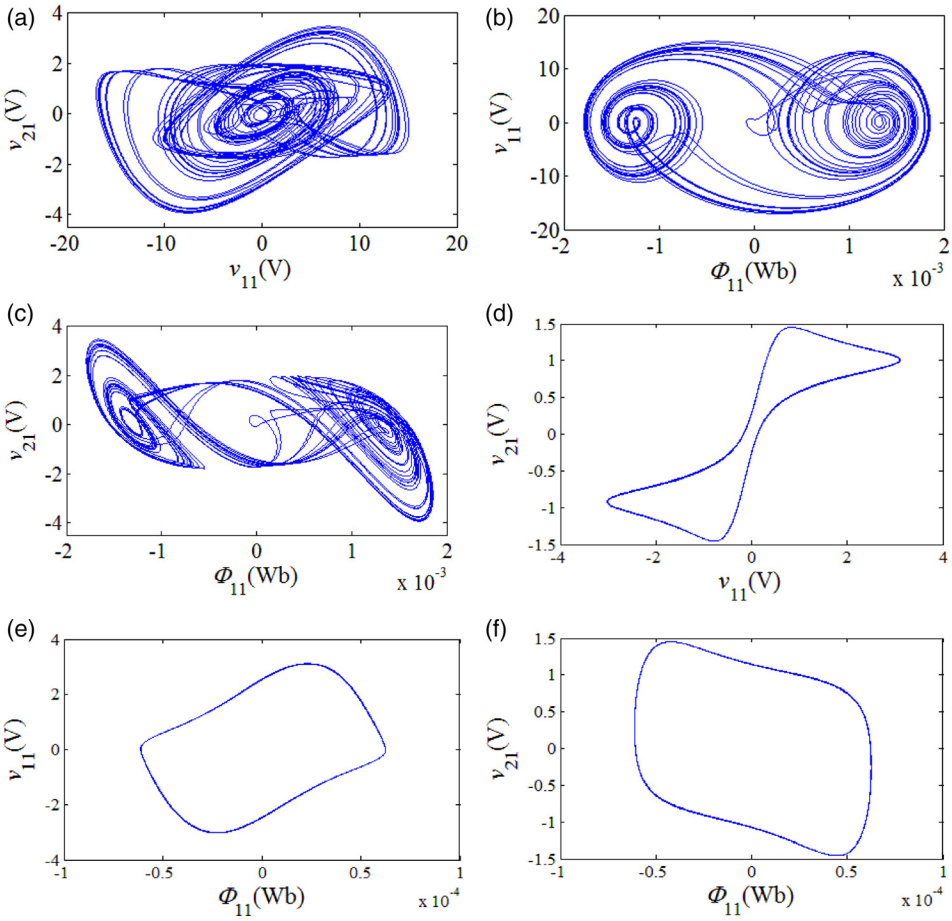

FIG. 7. Projections of typical chaotic orbits at $\kappa_1 = 10$ mS/Wb^2 on the (a) $v_{11} - v_{21}$ plane; (b) $\varphi_{11} - v_{11}$ plane; (c) $\varphi_{11} - v_{21}$ plane, as well as projections of periodic orbits at $\kappa_1 = 400$ mS/Wb^2 on the (d) $v_{11} - v_{21}$ plane; (e) $\varphi_{11} - v_{11}$ plane; and (f) $\varphi_{11} - v_{21}$ plane.

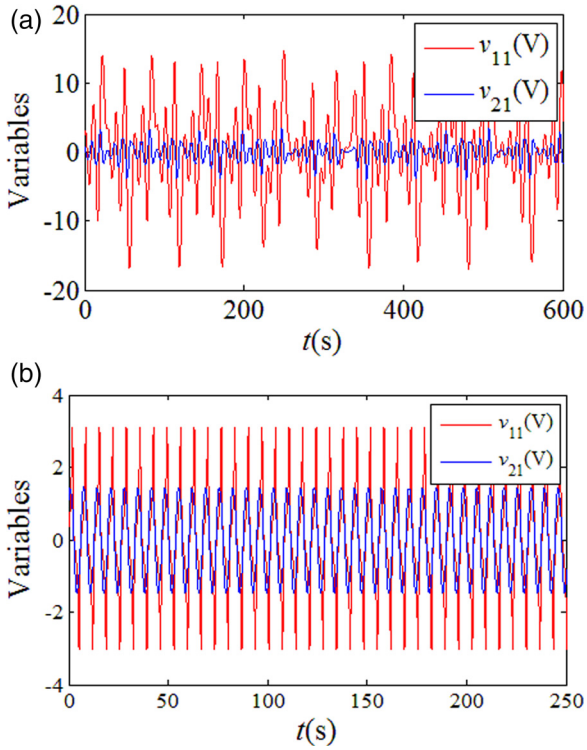

FIG. 8. Time-domain waveforms in the time interval [0 s, 250 s] when (a) the system is chaotic at $\kappa_1 = 10$ mS/Wb^2 and (b) the system is periodic at $\kappa_1 = 400$ S/Wb^2.

First, the circuit schematic of a new MR emulator is newly proposed in Fig. 10. The floating MR emulator is composed of four current feedback op-amps (CFOAs) AD844, two multipliers AD633, one amplifier TL084, eight resistors, and one capacitor. AD844 can perform as a current conveyor and voltage follower. The function of CFOAs U1 and U3 is to integrate the voltage difference between terminals A and B to an equivalent flux; the function of the multiplier U5 is to multiply flux by flux; the function of the op-amp U6 is to act as an inverting summing amplifier to add potential coupling information from another MR; AD633 is used to multiply the voltage output v_{u4} from U6 with the output v_{u1} from U1; CFOAs U2 and U4 are used to ensure that the current i_3 flowing through R_8 is equivalent to the current i_{MR} flowing through the MR emulator.

This MR emulator has two floating terminals A and B without a grounded restriction and can easily be connected with other circuit components in series. Note that, every MR will have a "coupling port," namely, the non-inverting $(+)$ pin of U61 and U62. In future research, multiple MR emulators can be connected through the coupling port via resistors to emulate multiple MRs coupled together.

With a single MR emulator presented, we shift our attention to the coupling action between two MRs. Figure 11 shows the schematic of two coupled MRs. It can be seen that this circuit is symmetrically structured by two MRs through the coupling connection (two red wires), which can be achieved by having two amplifiers U61 and U62 operating as analog adders. The operating principle of coupling is as follows. The voltage v_{u32} from MR2 can be connected to the non-inverting

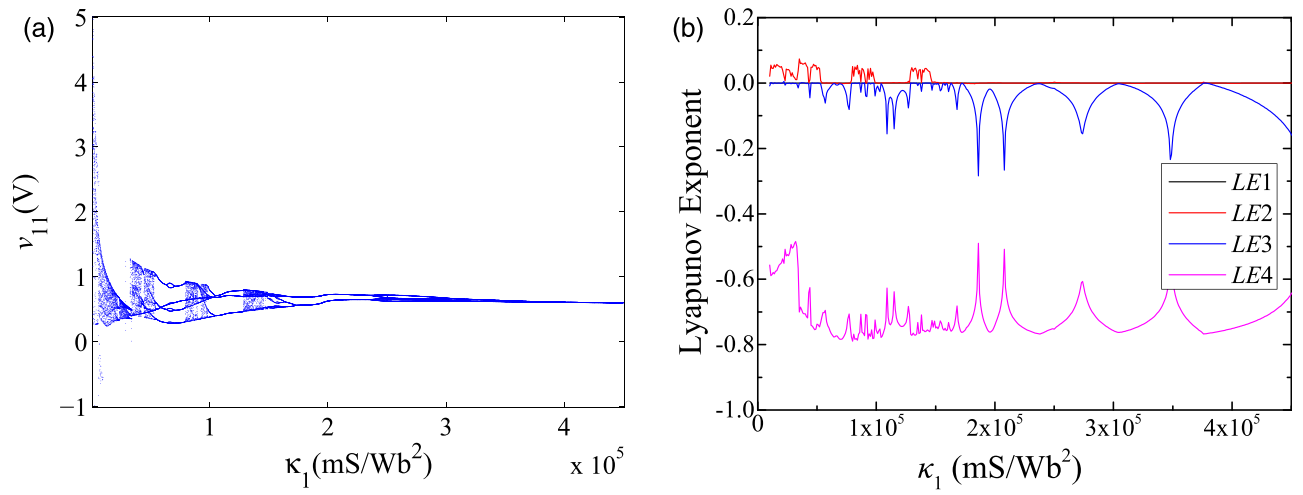

FIG. 9. Dynamical behaviors of the memristive circuit with κ_1 increasing: (a) bifurcation diagram with respect to κ_1 and (b) Lyapunov exponent spectrum with respect to κ_1.

pin of U61 through the resistor R_{41} to realize the coupling action from MR2 to MR1, and the voltage v_{u31} from MR1 to U62 through the resistor R_{41} to realize the coupling action from MR1 to MR2. The coupling action between two MRs is adjusted through adjusting coupling resistors R_{41} and R_{42}.

In this section, fluxes φ_{A1B1} and φ_{A2B2} are used to represent the time integral of terminal voltages v_{A1B1} and v_{A2B2} across MR1 and MR2, respectively.

According to circuit schematics in Figs. 10 and 11 and the datasheet of active chips used in these two figures, expressions for the equivalent memductance of MR emulators under different operating modes are listed as follows. Note that the full derivation of (22a), (22b), (23a), and (23b) are given in the Appendix.

First, the coupling strengths κ_1 and κ_2 are determined to be zero by connecting the coupling port of each MR, as shown in Fig. 10, to the ground. In this case, two MRs can perform independently to each other. By referring to Eqs. (A10) and (A11) in the Appendix, the memductance $W_1(\varphi_{A1B1})$ and $W_2(\varphi_{A2B2})$ can be expressed with

$$\begin{aligned} W_1 &= \frac{R_{21}R_{f1}(R_{61}+R_{71})\varphi_{A1B1}^2}{100R_{11}R_{31}R_{61}R_{81}(R_{11}C_{31})^2} - \frac{R_{21}}{R_{11}R_{81}} \\ &= \alpha_1\varphi_{A1B1}^2 + \beta_1, \end{aligned} \tag{22a}$$

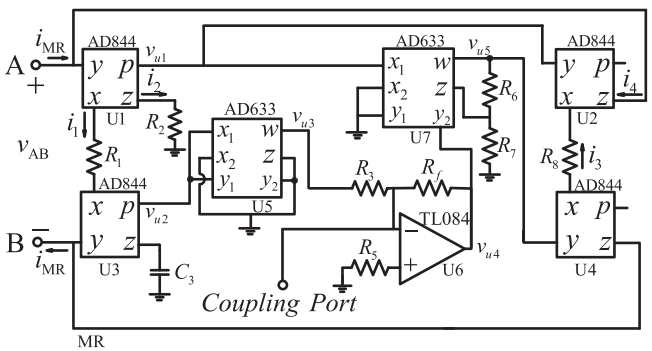

FIG. 10. Circuit schematic of a MR emulator with floating terminals and a coupling port.

$$\begin{aligned} W_2 &= \frac{R_{22}R_{f2}(R_{62}+R_{72})\varphi_{A2B2}^2}{100R_{12}R_{32}R_{62}R_{82}(R_{12}C_{32})^2} - \frac{R_{22}}{R_{12}R_{82}} \\ &= \alpha_2\varphi_{A2B2}^2 + \beta_2. \end{aligned} \tag{22b}$$

Then, the coupling action between the two MRs can be taken into consideration by connecting MR1 and MR2 as in Fig. 11. The coupling-influenced memductance $W_1(\varphi_{A1B1}, \varphi_{A2B2})$ and $W_2(\varphi_{A2B2}, \varphi_{A1B1})$ can be expressed as

$$\begin{aligned} W_1 &= \frac{R_{21}R_{f1}(R_{61}+R_{71})\varphi_{A1B1}^2}{100R_{11}R_{31}R_{61}R_{81}(R_{11}C_{31})^2} \\ &\quad + \frac{R_{21}R_{f1}(R_{61}+R_{71})\varphi_{A2B2}^2}{100R_{11}R_{41}R_{61}R_{81}(R_{12}C_{32})^2} - \frac{R_{21}}{R_{11}R_{81}} \\ &= \alpha_1\varphi_{A1B1}^2 + \kappa_1\varphi_{A2B2}^2 + \beta_1, \end{aligned} \tag{23a}$$

$$\begin{aligned} W_2 &= \frac{R_{22}R_{f2}(R_{62}+R_{72})\varphi_{A2B2}^2}{100R_{12}R_{32}R_{62}R_{82}(R_{12}C_{32})^2} \\ &\quad + \frac{R_{22}R_{f2}(R_{62}+R_{72})\varphi_{A1B1}^2}{100R_{12}R_{42}R_{62}R_{82}(R_{11}C_{31})^2} - \frac{R_{22}}{R_{12}R_{82}} \\ &= \alpha_2\varphi_{A2B2}^2 + \kappa_2\varphi_{A1B1}^2 + \beta_2. \end{aligned} \tag{23b}$$

In (22a), (22b), (23a), and (23b), parameters $\alpha_1, \alpha_2, \beta_1, \beta_2, \kappa_1$, and κ_2 are defined as

$$\begin{aligned} \alpha_1 &= \frac{R_{21}R_{f1}(R_{61}+R_{71})}{100R_{11}R_{31}R_{61}R_{81}(R_{11}C_{31})^2}, \\ \alpha_2 &= \frac{R_{22}R_{f2}(R_{62}+R_{72})}{100R_{12}R_{32}R_{62}R_{82}(R_{12}C_{32})^2}, \end{aligned} \tag{24}$$

$$\beta_1 = -\frac{R_{21}}{R_{11}R_{81}}, \quad \beta_2 = -\frac{R_{22}}{R_{12}R_{82}}, \tag{25}$$

$$\begin{aligned} \kappa_1 &= \frac{R_{21}R_{f1}(R_{61}+R_{71})}{100R_{21}R_{41}R_{61}R_{81}(R_{12}C_{32})^2}, \\ \kappa_2 &= \frac{R_{22}R_{f2}(R_{62}+R_{72})}{100R_{12}R_{42}R_{62}R_{82}(R_{11}C_{31})^2}. \end{aligned} \tag{26}$$

In (22a), (22b), (23a), and (23b), α_1 and α_2 are constants which determine the variation rates of memductance, β_1 and

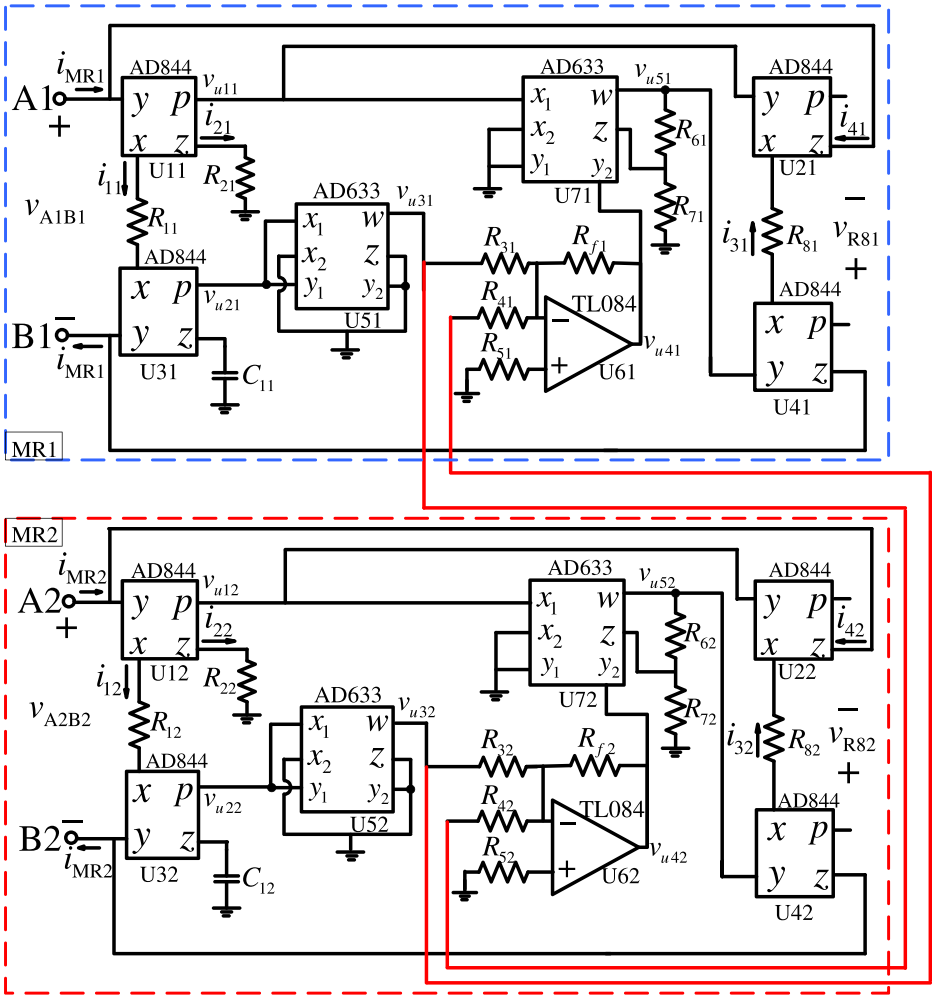

FIG. 11. Circuit schematic of two flux coupled MR emulators.

β_2 are regarded as the initial memductane values, κ_1 and κ_2 are adjustable constants which determine the coupling strength from MR2 to MR1 and MR1 to MR2, respectively. The unit of measurement for W_1 and W_2 is millisiemens (mS), and by adjusting R_{41} and R_{42}, the coupling strength between two MRs can be adjusted.

V. CIRCUIT IMPLEMENTATION IN PSpice AND SIMULATION RESULTS

The MR emulator adopted in this paper is a flux-controlled nonlinear resistor with cubic constitutive relation.

Based on the mathematical expression (A9) describing i_{MR1} in the Appendix, we can see that the value of current i_{MR1} is the same as i_{31}, which is proportional to the voltage across R_{81}. Thus, in this section, $-v_{R81}$ is measured in order to characterize $-i_{M1}$.

A. Single MR emulator

In order to demonstrate that the emulator presented successfully synthesizes a floating MR, we determined the $v-i$ curve of the MR emulator in a PSpice simulation. The simulation data was collected and then transferred into OriginPro8.0 software to plot the $v-i$ curves.

The circuit schematic for a single MR in Fig. 10 is adopted, and the simulation parameters are given as $C_3 = 80$ nF, $R_1 = 15\,\text{k}\Omega$, $R_2 = 60\,\text{k}\Omega$, $R_3 = 2\,\text{k}\Omega$, $R_f = R_5 = 1\,\text{k}\Omega$, $R_6 = 5\,\text{k}\Omega$, $R_7 = 28\,\text{k}\Omega$, and $R_8 = 3\,\text{k}\Omega$. According to (24) and (25), α and β can be calculated as $\alpha = 30.566$ mS/Wb^2 and $\beta = 1.333 \times 10^{-3}$ mS.

Figure 12 compares the measured hysteresis loops of the current and voltage of the circuit under the excitation of a sinusoidal input with amplitude of 1 V and frequencies of 50 and 75 Hz.

The corresponding pinched hysteresis loops of v_{A1B1} versus $-i_{M1}$ (represented by $-v_{R81}$) are confined to the first and the third quadrants of the $v_{A1B1} - (-v_{R81})$ plane, exhibiting a positive slope. This result demonstrates a successful synthesis of a MR emulator with negative resistance, thus allowing the two-terminal MR to act as an active device in chaotic circuit applications. The voltage-current characteristic passes together through the origin and is a pinched hysteresis loop that looks like an inclined "8." In particular, the pinched hysteresis loop shrinks and tends to a straight line as frequency increases, which is in accordance with Ref. 54. The simulation result shows a successful emulation of MR.

B. Coupled MR emulators

Then in order to test the feasibility of the proposed emulator to mimic the coupling action between two MRs, we simulated the circuit schematic in Fig. 11 and simulation parameters are given as $C_{31} = C_{32} = 80$ nF, $R_{11} = R_{12} = 15\,\text{k}\Omega$,

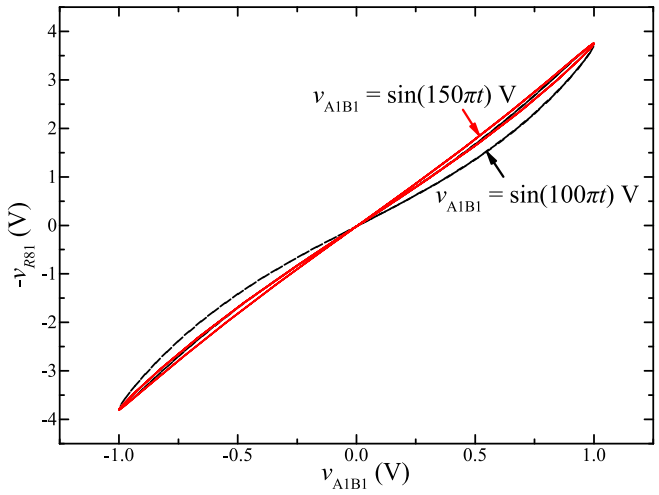

FIG. 12. Simulation results of pinched hysteresis loops for the MR emulator under different excitation voltages of $v_{A1B1} = \sin(100\pi t)$ V and $v_{A1B1} = \sin(150\pi t)$ V.

$R_{21} = R_{22} = 60\,\text{k}\Omega$, $R_{31} = R_{32} = 2\,\text{k}\Omega$, $R_{f1} = R_{f2} = R_{51} = R_{52} = 1\,\text{k}\Omega$, $R_{61} = R_{62} = 5\,\text{k}\Omega$, $R_{71} = R_{72} = 28\,\text{k}\Omega$, and $R_{81} = R_{82} = 3\,\text{k}\Omega$. R_{41} and R_{42} are two adjustable resistors. Parameters can be calculated according to (23a) and (23b) as $\alpha_1 = \alpha_2 = 30.566$ mS/Wb^2 and $\beta_1 = \beta_2 = 1.333 \times 10^{-3}$ mS. A sinusoidal voltage with 1 V amplitude and 50 Hz frequency is applied across A1 and B1, as well as A2 and B2, to excite MR1 and MR2. By adjusting the values of R_{41} and R_{42}, the coupling strength between two MRs can be altered without altering values of α and β. Figure 13(a) compares the $v_{A1B1} - (-v_{R81})$ loci for MR1 when it is uncoupled and coupled with MR2 respectively. When MRs are uncoupled, $\alpha = 30.566$ mS/Wb^2, $\beta = 1.333 \times 10^{-3}$ mS/Wb^2 and $\kappa_1 = \kappa_2 = 0$. When MRs are coupled with coupling resistors configured as $R_{41} = R_{42} = 5\,\text{k}\Omega$, values of α and β are the same and coupling strengths can be calculated as $\kappa_1 = \kappa_2 = 12.222$ mS/Wb^2. According to (A9) and (A14) in the Appendix, when the value of current flowing through MR1 is negative, the occurrence of the coupling action between MRs will make the absolute value of the current i_{MR1} smaller, which is in accordance with the trend in Fig. 13(a). Figure 13(b) compares the $v_{A1B1} - (-v_{R81})$ loci for MR1 when it is coupled with MR2 under different coupling strengths. Figure 13(b) shows the $v_{A1B1} - (-v_{R81})$ loci for MR1 when the coupling resistors are configured as $R_{41} = 3\,\text{k}\Omega$ and $R_{42} = 5\,\text{k}\Omega$, as well as $R_{41} = R_{42} = 5\,\text{k}\Omega$. When $R_{41} = 3\,\text{k}\Omega$ and $R_{42} = 5\,\text{k}\Omega$, the coupling strengths are calculated as $\kappa_1 = 20.370$ mS/Wb^2 and $\kappa_2 = 12.222$ mS/Wb^2; when $R_{41} = R_{42} = 5\,\text{k}\Omega$, the coupling strengths are calculated as $\kappa_1 = \kappa_2 = 12.222$ mS/Wb^2. It can be concluded that the coupling action and the coupling strength can influence the $v - i$ characteristic of MR. According to (A13), when the value of the current flowing through MR1 is negative, the increase in the coupling strength between MRs will make the absolute value of current i_{MR1} smaller, which is in accordance with the trend shown in Fig. 13(b).

It can be concluded that the emulator designed in Sec. IV can synthesize a floating MR and multiple emulators can be coupled. The coupling strength between MR emulators can be controlled through adjusting the value of the coupling resistors, and the change in the coupling strength from other MRs can change the characteristics of the MR being coupled.

VI. EXPERIMENTAL RESULTS

In the hardware experiment, memristive Chua's circuit based on coupled MRs is built by using the newly designed MR emulator. Measurement and analysis of the circuit were performed using oscilloscope Keysight DSOX2014A for the observation of the time series and phase portraits for the circuit.

Based on the mathematical expressions (A3) and (A9) describing φ_{A1B1} and i_{MR1} in the Appendix, we can see that flux φ_{A1B1} is proportional to the voltage across C_{31} and the value of current i_{MR1} is the same as i_{31}, which is proportional to the voltage $-v_{u21}$ across R_{81}. Thus, in this section, voltages $-v_{u21}$ and $-v_{R81}$ are employed to characterize φ_{A1B1} and $-i_{M1}$, respectively, in the hardware experiment.

A. Memristive Chua's circuit based on serially connected MRs

First, a memristive Chua's circuit based on coupled MRs connected in series with identical polarities is built and tested. The parameters for implementing this circuit are chosen as $L_1 = 13.6$ mH, $C_1 = 12$ nF, $C_2 = 247$ nF, $C_{31} = C_{32} = 78$ nF, $R_p = 1.319\,\text{k}\Omega$, $R_{11} = R_{12} = 15\,\text{k}\Omega$, $R_{21} = 9.8\,\text{k}\Omega$, $R_{22} = 59.4\,\text{k}\Omega$, $R_{31} = R_{32} = 2\,\text{k}\Omega$, $R_{f1} = R_{f2} = R_{51} = R_{52} = 1\,\text{k}\Omega$, $R_{61} = R_{62} = 8.2\,\text{k}\Omega$, $R_{71} = R_{72} = 30\,\text{k}\Omega$, and $R_{81} = R_{82} = 3\,\text{k}\Omega$. Parameters in (24) and (25) can be calculated as $\alpha_1 = 3.706$ mS/Wb^2, $\alpha_2 = 22.461$ mS/Wb^2, $\beta_1 = 2.178 \times 10^{-4}$ mS, and $\beta_2 = 1.32 \times 10^{-3}$ mS.

The one-to-one relationships between variables mentioned in Subsections III A and VI A are as follows. Here, v_{11}

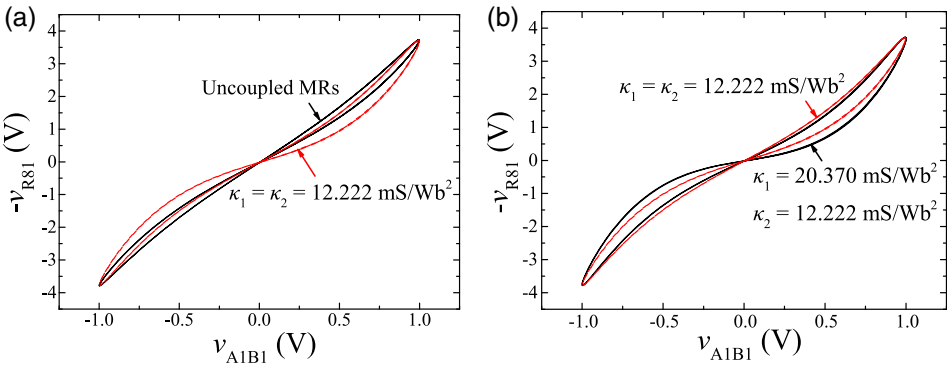

FIG. 13. Simulated pinched hysteresis loop curves for MR1 (a) when it is uncoupled and coupled with MR2; (b) when it is coupled with MR2 under different coupling strengths.

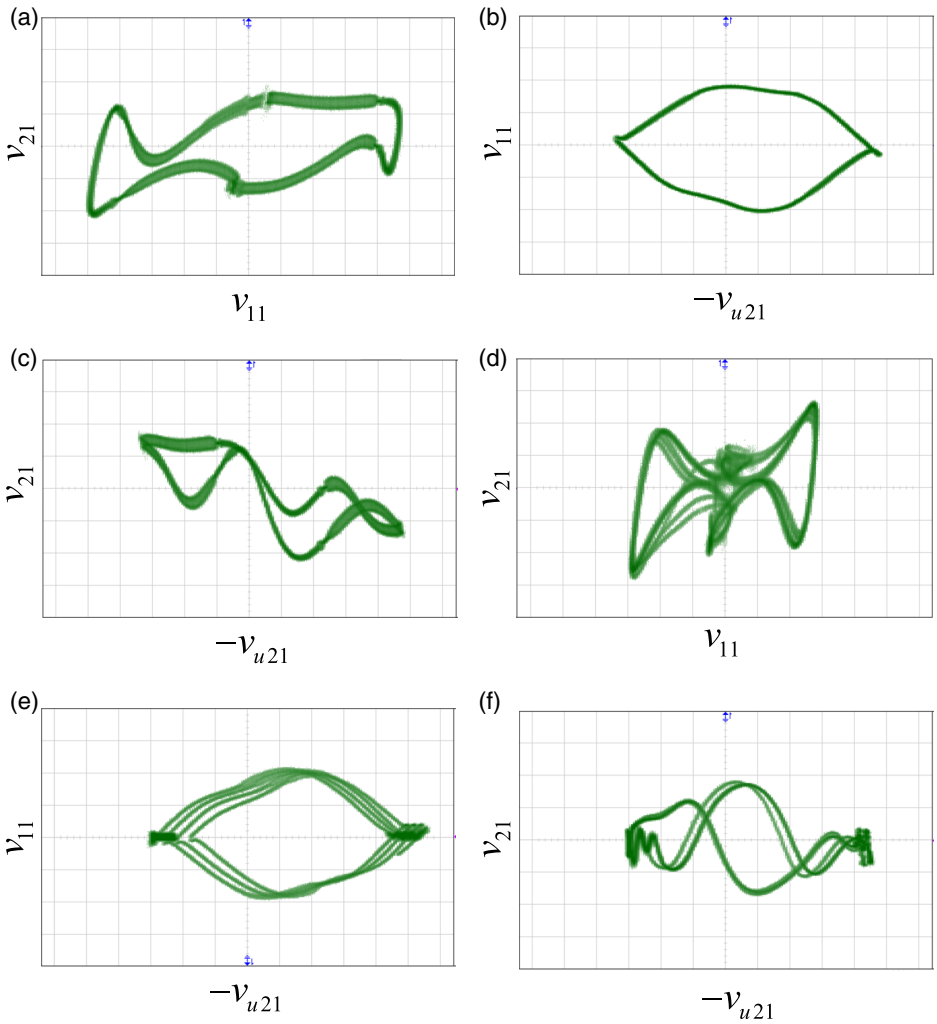

FIG. 14. Experimental phase portraits obtained from the circuit using an oscilloscope in the $X-Y$ mode: projections of periodic orbits at $\kappa_1 = 9.829$ mS/Wb^2 and $\kappa_2 = 44.921$ mS/Wb^2 on the (a) $v_{11} - v_{21}$ plane (x-axis: 2 V/div and y-axis: 500 mV/div); (b) $-v_{u21} - v_{11}$ plane (x-axis: 2V/div and y-axis: 5 V/div); (c) $-v_{u21} - v_{21}$ plane (x-axis: 2V/div and y-axis: 500 mV/div), as well as projections of typical chaotic attractor at $\kappa_1 = 46.320$ mS/Wb^2 and $\kappa_2 = 44.921$ mS/Wb^2 on the (d) $v_{11} - v_{21}$ plane (x-axis: 5 V/div and y-axis: 500 mV/div); (e) $-v_{u21} - v_{11}$ plane (x-axis: 2 V/div and y-axis: 5 V/div); and (f) $-v_{u21} - v_{21}$ plane (x-axis: 2 V/div and y-axis: 1 V/div).

is the voltage across the capacitor C_1, v_{21} is the voltage across the capacitor C_2, and i_L is the current flowing through the inductor L_1. The voltage $-v_{u21}$ is used to represent the flux φ_1, which equals φ_{A1B1}, the time integral of the voltage v_{A1B1} across MR1. Similarly, the voltage $-v_{u22}$ is used to represent φ_2, which equals φ_{A2B2}, the time integral of v_{A2B2}.

The initial values for the system variables shown in (14) is set as $(\varphi_1, \varphi_2, v_{11}, v_{21}, i_L) = (0, 0, 0, 0, 0)$.

By tuning the value of R_{41}, the coupling strength κ_1 can be altered, and the corresponding value of κ_1 is the bifurcation parameter. Some typical orbits of the system are measured in the $X-Y$ mode in Fig. 14, showing phase portraits of v_{11} versus v_{21}, φ_1 (represented by $-v_{u21}$) versus v_{11}, as well as $-v_{u21}$ versus v_{21}. Figures 14(a)–14(c) are measured using $R_{41} = 0.754\,\text{k}\Omega$ and $R_{42} = 1\,\text{k}\Omega$ [according to (26), $\kappa_1 = 9.829$ mS/Wb^2 and $\kappa_2 = 44.921$ mS/Wb^2], showing periodic-1 shapes. Figures 14(d)–14(f) present the measured chaotic attractors at $R_{41} = 0.159\,\text{k}\Omega$, $R_{42} = 1\,\text{k}\Omega$ ($\kappa_1 = 46.320$ mS/Wb^2 and $\kappa_2 = 44.921$ mS/Wb^2) and these phase portraits show chaotic traces.

The scopes are then placed into "freeze" mode for capturing corresponding time-domain waveforms of variables v_{11}, v_{21}, and φ_1 ($-v_{u21}$ instead) in periodic and chaotic states which are shown in Fig. 15. This demonstrates that the memristive Chua's circuit based on coupled MRs connected in series is capable of generating both chaotic signals and periodic signals under varying conditions of the memristive coupling strength.

B. Memristive Chua's circuit based on parallel connected MR

A memristive Chua's circuit based on coupled MRs connected in parallel with identical polarities is built and tested. The parameters for implementing this circuit are chosen as $L_1 = 18$ mH, $C_1 = 6.8$ nF, $C_2 = 68$ nF, $C_{31} = C_{32} = 110$ nF, $R_p = 1.319\,\text{k}\Omega$, $R_{11} = R_{12} = 15\,\text{k}\Omega$, $R_{21} = 60.5\,\text{k}\Omega$, $R_{22} = 36.7\,\text{k}\Omega$,

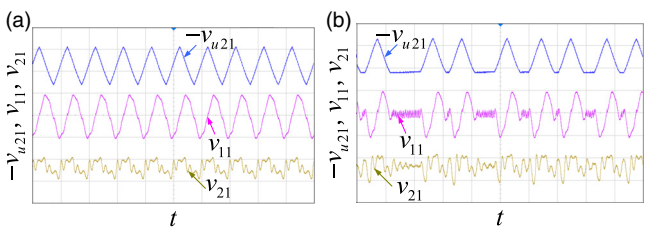

FIG. 15. Time-domain waveforms when (a) the system is periodic at $\kappa_1 = 9.829$ mS/Wb^2 and $\kappa_2 = 44.921$ mS/Wb^2; (b) the system is chaotic at $\kappa_1 = 46.320$ mS/Wb^2 and $\kappa_2 = 44.921$ mS/Wb^2. The scales are $X = 2$ ms/div, $Y = 10$ V/div, 10 V/div, and 1 V/div for $-v_{u21}$ (top waveform), v_{11} (middle waveform), and v_{21} (bottom waveform), respectively.

$R_{31} = R_{32} = 2\,\text{k}\Omega$, $R_{f1} = R_{f2} = R_{51} = R_{52} = 1\,\text{k}\Omega$, $R_{61} = R_{62} = 8.2\,\text{k}\Omega$, $R_{71} = R_{72} = 30\,\text{k}\Omega$, and $R_{81} = R_{82} = 5\,\text{k}\Omega$. Parameters in (24) and (25) can be calculated as $\alpha_1 = 6.902$ mS/Wb^2, $\alpha_2 = 4.187$ mS/Wb^2, $\beta_1 = 8.067 \times 10^{-4}$ mS, and $\beta_2 = 4.893 \times 10^{-4}$ mS.

The one-to-one relationships between variables mentioned in Subsections III C and VI B are as follows. v_{11} is the voltage across the capacitor C_1, v_{21} is the voltage across the capacitor C_2, and i_L is the current flowing through the inductor L_1. The voltage $-v_{u21}$ is used to represent φ_{11}, which equals φ_{A1B1} and φ_{A2B2}, the time integrals of the voltage v_{A1B1} across MR1 and the voltage v_{A2B2} across MR2, respectively.

The initial values for the system variables shown in (21) are set as $(\varphi_{11}, v_{11}, v_{21}, i_L) = (0, 0, 0, 0)$.

By tuning the value of R_{41}, the coupling strength κ_1 can be altered, and the corresponding value of κ_1 is the bifurcation parameter. Some typical orbits of the system are measured in the $X - Y$ mode in Fig. 16, showing phase portraits of v_{11} versus v_{21}, φ_{11} ($-v_{u21}$ instead) versus v_{11}, as well as φ_{11} versus v_{21}, respectively. Figures 16(a)–16(c) are measured chaotic attractors under $R_{41} = 0.746\,\text{k}\Omega$, $R_{42} = 0.746\,\text{k}\Omega$ [according to (26), $\kappa_1 = 18.067$ mS/Wb^2 and $\kappa_2 = 10.960$ mS/Wb^2], showing chaotic traces. Figures 16(d)–16(f) are measured at $R_{41} = 0.225\,\text{k}\Omega$ and $R_{42} = 0.746\,\text{k}\Omega$ ($\kappa_1 = 61.347$ mS/Wb^2 and $\kappa_2 = 10.960$ mS/Wb^2) and these phase portraits show periodic-1 shapes.

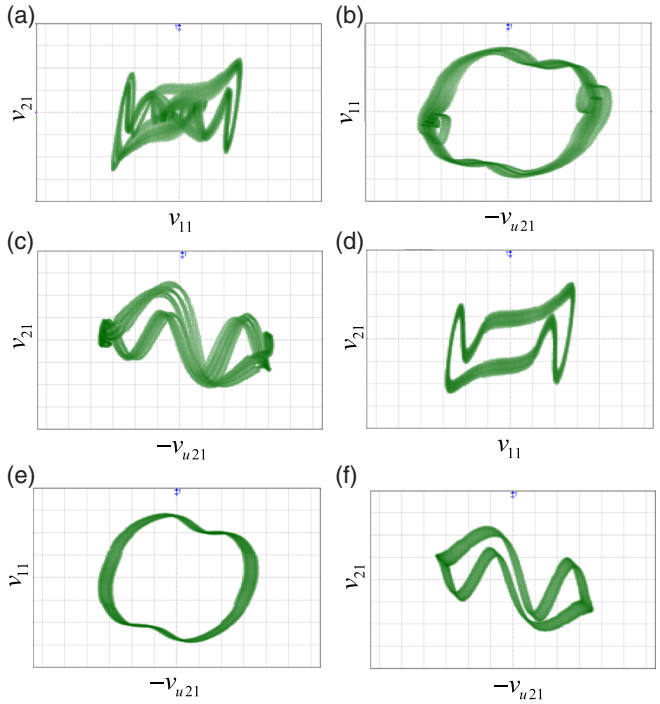

FIG. 16. Experimental phase portraits obtained from the circuit using an oscilloscope in the $X - Y$ mode: projections of typical chaotic attractor at $\kappa_1 = 18.067$ mS/Wb^2 and $\kappa_2 = 10.960$ mS/Wb^2 on the (a) $v_{11} - v_{21}$ plane (x-axis: 5 V/div and y-axis: 1 V/div); (b) $-v_{u21} - v_{11}$ plane (x-axis: 1 V/div and y-axis: 5 V/div); (c) $-v_{u21} - v_{21}$ plane (x-axis: 1 V/div and y-axis: 1 V/div), as well as projections of periodic orbits at $\kappa_1 = 61.347$ mS/Wb^2 and $\kappa_2 = 10.960$ mS/Wb^2 on the (d) $v_{11} - v_{21}$ plane (x-axis: 5 V/div and y-axis: 1 V/div); (e) $-v_{u21} - v_{11}$ plane (x-axis: 1 V/div and y-axis: 5 V/div); and (f) $-v_{u21} - v_{21}$ plane (x-axis: 1 V/div and y-axis: 1 V/div).

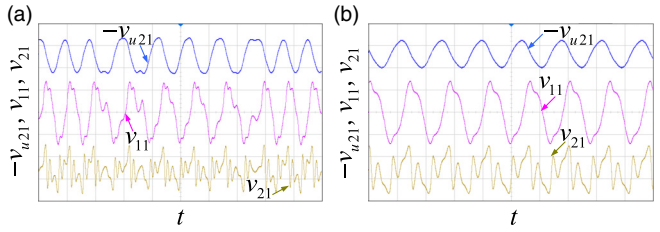

FIG. 17. Time-domain waveforms when (a) the system is chaotic at $\kappa_1 = 18.067$ mS/Wb^2 and $\kappa_2 = 10.960$ mS/Wb^2; (b) the system is periodic at $\kappa_1 = 61.347$ mS/Wb^{2}and $\kappa_2 = 10.960$ mS/Wb^2. The scales are $X = 5$ ms/div, $Y = 10$ V/div, 10 V/div, and 1 V/div for $-v_{u21}$ (top waveform), v_{11} (middle waveform), and v_{21} (bottom waveform), respectively.

The corresponding time-domain waveforms of variables φ_{11} ($-v_{u21}$ instead), v_{11}, and v_{21} in periodic and chaotic states are shown in Fig. 17, which demonstrates that the memristive Chua's circuit based on coupled MRs connected in parallel is able to generate chaotic signals or periodic signals under different conditions of the coupling strength between MRs.

Additionally, we have tested pinched hysteresis loops of v_{A1B1} versus $(-i_{M1})$ ($-v_{R81}$ instead) loci of the MR emulator during periodic and chaotic oscillations in Fig. 18 with circuit parameters configured the same as those at the beginning of this subsection, showing pinched hysteresis loops for MRs under period-1 and chaotic circumstances. In these two circumstances, the voltage and the negative current pass together through the origin, and pinched hysteresis loops for these two circumstances are confined to the first and the third quadrants of the $v - i$ plane, which demonstrates a successful synthesis of a MR emulator with negative resistance.

When compared to the parameters used in simulations, parameters used in the hardware experiment also show the feasibility and robustness to couple MRs with different α and β values. Even if two MRs have different variation rates of memductance and different initial memductance values, they can be coupled together and operate successfully.

We can see from the experimental results in Sec. VI that the change in dynamical behaviors of memristive Chua's circuits containing two compositely connected MR emulators with respect to different values of the coupling strength κ_1 is in good agreement with the trend in the simulations provided in Sec. III, validating the effective influence of adjusting the coupling strength between MRs on circuit dynamics. It is also concluded that in the hardware experimental process of designing applications containing densely spaced MRs, it is

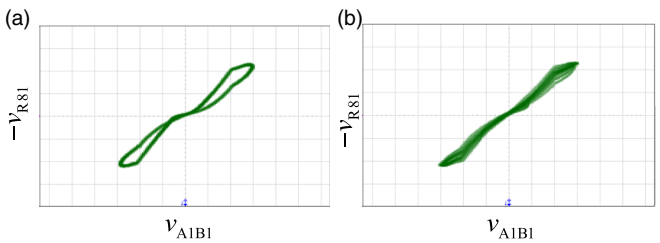

FIG. 18. The loci of v_{A1B1} versus $-v_{R81}$ projected onto the v vs. i plane during (a) periodic oscillations and (b) chaotic oscillations. The scales are $X = 5$ V/div and $Y = 5$ V/div.

necessary to consider the coupling action between MRs to accurately describe dynamical responses of MRs-based circuits and systems.

VII. CONCLUSION

The study presented in this paper examined the potential interaction, namely, the memristive coupling behavior between MRs about how the memristive coupling behavior can influence the system dynamics of memristive chaotic circuits. Until now, the interaction, especially the coupling behavior between closely placed MRs has been largely ignored while designing MRs-based circuits. This work considers the fundamental memristive coupling parameter that has previously been ignored for the generation and tuning of chaos in MRs-based circuits. Special cases of two coupled MRs connected in series and parallel are used in Chua's circuit for demonstration, the methodology of which can also be treated as a typical example for analyzing the research on future circuits containing multiple MRs within close physical proximity to each other. It is important to integrate the memristive coupling effect into the process of memristive circuit designing in simulations and hardware experiments in order to see how the coupling will affect the circuit dynamical responses, especially for those circuits that require accurate or specific types of circuit responses, rather than as an afterthought or remedy to compensate for some undesired or unexpected performance from a memristive circuit.

Simulations in MATLAB and PSpice are verified via hardware experimentation by using a newly presented, successfully fabricated flux-controlled floating MR emulator. Multiple emulators can be coupled together, whilst this paper purely focuses on the use of a pair of flux-controlled MRs as a typical example to analyze. Simulations and hardware experiments are in good agreement. The system dynamic routes of the memristive Chua's circuit for different occasions when MRs connected in series or parallel under specific parameters configuration are analyzed, concluding that by tuning the coupling strength between MRs, the coupling effect will influence circuit dynamical responses of MRs-based circuits. Despite emphasizing the importance to consider the coupling action between MRs while designing circuits to avoid undesirable circuit responses and mitigate if necessary, this work may be further applied in any field which utilizes chaotic circuits, such as the use in image encryption, secure digital communication, neural engineering, and so forth.

The study in this paper furthers our fundamental understanding of memristive dynamics, as we present a new possible way of tuning chaos within a system by altering the coupling strength between a pair of MRs. Future research may explore the coupling action between more than two MRs or between MRs and other circuit components with intrinsic coupling action, such as capacitors and inductors with capacitive and inductive coupling effects, respectively.

APPENDIX: DERIVATION OF MEMDUCTANCE VALUES

The derivation of Eqs. (22a), (22b), (23a), and (23b) are given in the Appendix. In light of the symmetry between two coupled MR emulators, only the upper MR emulator is taken for demonstration with respect to Fig. 11. According to the data sheet of the CFOA AD844, the voltage of the x pin follows the y pin, the voltage of the p pin follows the z pin, and the current flowing into the z pin follows the current flowing into through the x pin. No current is flowing into pin y. When the terminal voltage across A1 and B1 is denoted as v_{A1B1}, the current flowing through R_{11} can be expressed as

$$i_{11} = \frac{v_{A1B1}}{R_{11}}. \tag{A1}$$

When the circuit is working at time t, the charge flowing through C_{31} can be calculated as

$$Q_{C_{31}} = \int_0^t i_{11} = \frac{\varphi_{A1B1}}{R_{11}}, \tag{A2}$$

where φ_{A1B1} is the time integration of the terminal voltage v_{A1B1}.

The voltage across the capacitor C_{31} can be expressed as

$$v_{u21} = -\frac{\varphi_{A1B1}}{R_{11}C_{31}}. \tag{A3}$$

The current flowing through R_{21} can be calculated as

$$i_{21} = i_{11} = \frac{v_{A1B1}}{R_{11}}. \tag{A4}$$

The output voltage of the p pin of AD844-U11 can be calculated as

$$v_{u11} = i_{21} \times R_{21} = \frac{v_{A1B1}R_{21}}{R_{11}}. \tag{A5}$$

According to the data sheet of AD633, the output voltage of the w pin of AD633-U51 can be expressed as

$$v_{u31} = \frac{v_{u21}^2}{10} = \frac{\varphi_{A1B1}^2}{10(R_{11}C_{31})^2}. \tag{A6}$$

First, the coupling strengths κ_1 and κ_2 are determined to be zero by connecting the left terminals of resistors R_{14} and R_{24} to the ground. In this case, two MRs can perform independently from each other.

The op-amp TL084-U61, as well as resistors R_{31}, R_{51}, R_{f1} make up an inverting summing amplifier. The output voltage v_{u41} can be expressed as

$$v_{u41} = -\frac{R_{f1}}{R_{31}} = -R_{f1}\left[\frac{\varphi_{A1B1}^2}{10R_{31}(R_{11}C_{31})^2}\right]. \tag{A7}$$

The output voltage of AD633-U71 can be expressed as

$$\begin{aligned} v_{u51} &= \frac{v_{u11}v_{u41}}{10}\frac{(R_{61}+R_{71})}{R_{61}} \\ &= \frac{R_{21}R_{f1}(R_{61}+R_{71})v_{A1B1}\varphi_{A1B1}^2}{100R_{11}R_{31}R_{61}(R_{11}C_{31})^2}. \end{aligned} \tag{A8}$$

As no current is flowing into pin y of AD844, the current i_{MR1} flowing into the terminal A1 will flow directly through z pins of AD844-U21 and AD844-U41, rather than z pins of

AD844-U11 and AD844-U31. Thus, the current flowing through R_{81} can be calculated as

$$i_{31} = i_{41} = i_{MR1} = \frac{v_{u51} - v_{u11}}{R_{81}} = v_{A1B1}\left[\frac{R_{21}R_{f1}(R_{61}+R_{71})\varphi_{A1B1}^2}{100R_{11}R_{31}R_{61}R_{81}(R_{11}C_{31})^2} - \frac{R_{21}}{R_{11}R_{81}}\right]. \quad \text{(A9)}$$

The memductance $W_1(\varphi_{A1B1})$ can be expressed as

$$W_1 = \frac{i_{MR1}}{v_{A1B1}} = \frac{R_{21}R_{f1}(R_{61}+R_{71})\varphi_{A1B1}^2}{100R_{11}R_{31}R_{61}R_{81}(R_{11}C_{31})^2} - \frac{R_{21}}{R_{11}R_{81}} = \alpha_1\varphi_{A1B1}^2 + \beta_1. \quad \text{(A10)}$$

Similarly, the memductance $W_2(\varphi_{A2B2})$ can be expressed as

$$W_2 = \frac{R_{22}R_{f2}(R_{62}+R_{72})\varphi_{A2B2}^2}{100R_{12}R_{32}R_{62}R_{82}(R_{12}C_{32})^2} - \frac{R_{22}}{R_{12}R_{82}} = \alpha_2\varphi_{A2B2}^2 + \beta_2. \quad \text{(A11)}$$

The expressions of α_1, α_2, β_1, and β_2 shown in Eqs. (A10) and (A11) are listed in (A17) and (A18) followed with the explanation of their meanings.

The coupling action between two MRs is then taken into consideration by using coupling ports. The w terminal of AD633-U52 from MR2 can be connected to the coupling port of MR1 through the resistor R_{41}, and the w terminal of AD633-U51 from MR1 can be connected to the coupling port of MR2 through the resistor R_{41}. Considering the coupling action, the output voltage v_{u41} of TL084-U61 can be expressed as

$$v_{u41} = -R_{f1}\left[\frac{\varphi_{A1B1}^2}{10R_{31}(R_{11}C_{31})^2} + \frac{\varphi_{A2B2}^2}{10R_{41}(R_{12}C_{32})^2}\right]. \quad \text{(A12)}$$

The output v_{u51} of AD633-U71 can be calculated as

$$v_{u51} = \frac{R_{21}R_{f1}(R_{61}+R_{71})v_{A1B1}}{100R_{11}R_{61}} \times \left[\frac{\varphi_{A1B1}^2}{R_{31}(R_{11}C_{31})^2} + \frac{\varphi_{A2B2}^2}{R_{41}(R_{12}C_{32})^2}\right]. \quad \text{(A13)}$$

The current flowing through MR1 can be calculated as

$$i_{31} = v_{A1B1}\left[\frac{R_{21}R_{f1}(R_{61}+R_{71})\varphi_{A1B1}^2}{100R_{11}R_{31}R_{61}R_{81}(R_{11}C_{31})^2} + \frac{R_{21}R_{f1}(R_{61}+R_{71})\varphi_{A1B1}^2}{100R_{11}R_{41}R_{61}R_{81}(R_{12}C_{32})^2} - \frac{R_{21}}{R_{11}R_{81}}\right]. \quad \text{(A14)}$$

The memductance $W_1(\varphi_{A1B1}, \varphi_{A2B2})$ can be calculated as

$$W_1 = \frac{R_{21}R_{f1}(R_{61}+R_{71})\varphi_{A1B1}^2}{100R_{11}R_{31}R_{61}R_{81}(R_{11}C_{31})^2} + \frac{R_{21}R_{f1}(R_{61}+R_{71})\varphi_{A2B2}^2}{100R_{11}R_{41}R_{61}R_{81}(R_{12}C_{32})^2} - \frac{R_{21}}{R_{11}R_{81}} = \alpha_1\varphi_{A1B1}^2 + \kappa_1\varphi_{A2B2}^2 + \beta_1. \quad \text{(A15)}$$

Similarly, the memductance $W_2(\varphi_{A2B2}, \varphi_{A1B1})$ can be calculated as

$$W_2 = \frac{R_{22}R_{f2}(R_{62}+R_{72})\varphi_{A2B2}^2}{100R_{12}R_{32}R_{62}R_{82}(R_{12}C_{32})^2} + \frac{R_{22}R_{f2}(R_{62}+R_{72})\varphi_{A1B1}^2}{100R_{12}R_{42}R_{62}R_{82}(R_{11}C_{31})^2} - \frac{R_{22}}{R_{12}R_{82}} = \alpha_2\varphi_{A2B2}^2 + \kappa_2\varphi_{A1B1}^2 + \beta_2. \quad \text{(A16)}$$

In Eqs. (A10), (A11), (A15), and (A16), α_1 and α_2 are constants which determine the variation rates of memductance, β_1 and β_2 are regarded as the initial memductane values, κ_1 and κ_2 are adjustable constants which determine the coupling strength from MR2 to MR1 and MR1 to MR2, respectively. The unit of measurement for W_1 and W_2 is millisiemens (mS)

$$\alpha_1 = \frac{R_{21}R_{f1}(R_{61}+R_{71})}{100R_{11}R_{31}R_{61}R_{81}(R_{11}C_{31})^2}, \quad \alpha_2 = \frac{R_{22}R_{f2}(R_{62}+R_{72})}{100R_{12}R_{32}R_{62}R_{82}(R_{12}C_{32})^2}, \quad \text{(A17)}$$

$$\beta_1 = -\frac{R_{21}}{R_{11}R_{81}}, \quad \beta_2 = -\frac{R_{22}}{R_{12}R_{82}}, \quad \text{(A18)}$$

$$\kappa_1 = \frac{R_{21}R_{f1}(R_{61}+R_{71})}{100R_{21}R_{41}R_{61}R_{81}(R_{12}C_{32})^2}, \quad \kappa_2 = \frac{R_{22}R_{f2}(R_{62}+R_{72})}{100R_{12}R_{42}R_{62}R_{82}(R_{11}C_{31})^2}. \quad \text{(A19)}$$

[1]L. Chua, "Memristor: The missing circuit element," IEEE Trans. Circuit Theory **18**(5), 507–519 (1971).

[2]D. B. Strukov, G. S. Snider, D. R. Stewart, and R. S. Williams, "The missing memristor found," Nature **453**(7191), 80–83 (2008).

[3]S. Park, M. Chu, J. Kim, J. Noh, M. Jeon, B. Hun Lee, H. Hwang, B. Lee, and B-g Lee, "Electronic system with memristive synapses for pattern recognition," Sci. Rep. **5**, 10123 (2015).

[4]I. Gupta, A. Serb, A. Khiat, R. Zeitler, S. Vassanelli, and T. Prodromakis, "Real-time encoding and compression of neuronal spikes by metal-oxide memristors," Nat. Commun. **7**, 12805 (2016).

[5]C. Wang, M. Lv, A. Alsaedi, and J. Ma, "Synchronization stability and pattern selection in a memristive neuronal network," Chaos **27**(11), 113108 (2017).

[6]C. Yakopcic, T. M. Taha, and M. McLean, "Method for ex-situ training in memristor-based neuromorphic circuit using robust weight programming method," Electron. Lett. **51**(12), 899–900 (2015).

[7]Y. Chang, F. Zhou, B. W. Fowler, Y. Chen, C.-C. Hsieh, L. Guckert, E. E. Swartzlander, and J. C. Lee, "Memcomputing (memristor plus computing) in intrinsic SiO_x-based resistive switching memory: Arithmetic operations for logic applications," IEEE Trans. Electron Devices **64**(7), 2977–2983 (2017).

[8]K. M. Kim, J. Zhang, C. Graves, J. J. Yang, B. J. Choi, C. S. Hwang, Z. Li, and R. S. Williams, "Low-power, self-rectifying, and forming-free memristor with an asymmetric programing voltage for a high-density crossbar application," Nano Lett. **16**(11), 6724–6732 (2016).

[9]F. L. Traversa and M. Di Ventra, "Polynomial-time solution of prime factorization and NP-complete problems with digital memcomputing machines," Chaos **27**(2), 023107 (2017).

[10]D. Chabi, Z. Wang, C. Bennett, J.-O. Klein, and W. Zhao, "Ultrahigh density memristor neural crossbar for on-chip supervised learning," IEEE Trans. Nanotechnol. **14**(6), 954–962 (2015).

[11]B. Chakrabarti, M. A. Lastras-Montano, G. Adam, M. Prezioso, B. Hoskins, K.-T. Cheng, and D. B. Strukov, "A multiply-add engine with monolithically integrated 3D memristor crossbar/CMOS hybrid circuit," Sci. Rep. **7**, 42429 (2017).

[12]S. Benderli and T. A. Wey, "On spice macromodelling of TiO_2 memristors," Electron. Lett. **45**(7), 377–379 (2009).

[13]Á. Rák and G. Cserey, "Macromodeling of the memristor in spice," IEEE Trans. Comput.-Aided Des. Integr. Circuits Syst. **29**(4), 632–636 (2010).

[14]S. Shin, K. Kim, and S.-M. Kang, "Compact models for memristors based on charge-flux constitutive relationships," IEEE Trans. Comput.-Aided Des. Integr. Circuits Syst. **29**(4), 590–598 (2010).

[15]H. Kim, M. P. Sah, C. Yang, S. Cho, and L. O. Chua, "Memristor emulator for memristor circuit applications," IEEE Trans. Circuits Syst. I: Reg. Pap. **59**(10), 2422–2431 (2012).

[16]R. K. Budhathoki, M. P. D. Sah, C. Yang, H. Kim, and L. Chua, "Transient behaviors of multiple memristor circuits based on flux charge relationship," Int. J. Bifurcation Chaos **24**(02), 1430006 (2014).

[17]R. K. Budhathoki, M. P. Sah, S. P. Adhikari, H. Kim, and L. Chua, "Composite behavior of multiple memristor circuits," IEEE Trans. Circuits Syst. I: Reg. Pap. **60**(10), 2688–2700 (2013).

[18]L. V. Gambuzza, A. Buscarino, L. Fortuna, and M. Frasca, "Memristor-based adaptive coupling for consensus and synchronization," IEEE Trans. Circuits Syst. I: Reg. Pap. **62**(4), 1175–1184 (2015).

[19]Y. Zhou, Y. Li, L. Xu, S. Zhong, H. Sun, and X. Miao, "16 Boolean logics in three steps with two anti-serially connected memristors," Appl. Phys. Lett. **106**(23), 233502 (2015).

[20]J. Rajendran, R. Karri, and G. S. Rose, "Improving tolerance to variations in memristor-based applications using parallel memristors," IEEE Trans. Comput. **64**(3), 733–746 (2015).

[21]P. Meuffels and R. Soni, "Fundamental issues and problems in the realization of memristors," preprint arXiv:1207.7319 (2012).

[22]W. Cai and R. Tetzlaff, "Beyond series and parallel: Coupling as a third relation in memristive systems," in *IEEE International Symposium on Circuits and Systems (ISCAS)* (IEEE, 2014), pp. 1259–1262.

[23]W. Yan, Y. Jiu, W. Li-Dan, and D. Shu-Kai, "Research of coupling behavior based on series-parallel flux-controlled memristor," Acta Phys. Sin. **64**(23), 0237303 (2015).

[24]D. Yu, H. H. Ching Iu, Y. Liang, T. Fernando, and L. O. Chua, "Dynamic behavior of coupled memristor circuits," IEEE Trans. Circuits Syst. I: Reg. Pap. **62**(6), 1607–1616 (2015).

[25]S. Li, D. Yu, H. Chen, H. Cheng, and X. Zan, "Spontaneous synchronization of two Chua's circuits based on coupled memristors," in 14th International Conference on Control, Automation, Robotics and Vision (ICARCV) (IEEE, 2016), pp. 1–4.

[26]J. K. Eshraghian, H. H. Ching Iu, T. Fernando, D. Yu, and Z. Li, "Modelling and characterization of dynamic behavior of coupled memristor circuits," in *IEEE International Symposium on Circuits and Systems (ISCAS)* (IEEE, 2016), pp. 690–693.

[27]D. Yu, C. Zheng, H. H. Ching Iu, T. Fernando, and L. O. Chua, "A new circuit for emulating memristors using inductive coupling," IEEE Access **5**, 1284–1295 (2017).

[28]V. Mladenov and S. Kirilov, "Analysis of the mutual inductive and capacitive connections and tolerances of memristors parameters of a memristor memory matrix," in *European Conference on Circuit Theory and Design (ECCTD)* (IEEE, 2013), pp. 1–4.

[29]A. C. Torrezan, J. P. Strachan, G. Medeiros-Ribeiro, and R. Stanley Williams, "Sub-nanosecond switching of a tantalum oxide memristor," Nanotechnology **22**(48), 485203 (2011).

[30]M. P. Sah, C. Yang, H. Kim, B. Muthuswamy, J. Jevtic, and L. Chua, "A generic model of memristors with parasitic components," IEEE Trans. Circuits Syst. I: Reg. Pap. **62**(3), 891–898 (2015).

[31]B. Muthuswamy, J. Jevtic, H. H. Ching Iu, C. K. Subramaniam, K. Ganesan, V. Sankaranarayanan, K. Sethupathi, H. Kim, M. P. Shah, and L. O. Chua, "Memristor modelling," in *IEEE International Symposium on Circuits and Systems (ISCAS)* (IEEE, 2014), pp. 490–493.

[32]B. Bao, H. Bao, N. Wang, M. Chen, and Q. Xu, "Hidden extreme multistability in memristive hyperchaotic system," Chaos, Solitons Fractals **94**, 102–111 (2017).

[33]A. L. Fitch, D. Yu, H. H. Ching Iu, and V. Sreeram, "Hyperchaos in a memristor-based modified canonical Chua's circuit," Int. J. Bifurcation Chaos **22**(06), 1250133 (2012).

[34]W. Hu, D. Ding, and N. Wang, "Nonlinear dynamic analysis of a simplest fractional-order delayed memristive chaotic system," J. Comput. Nonlinear Dyn. **12**(4), 041003 (2017).

[35]J. Kengne, A. Nguomkam Negou, and D. Tchiotsop, "Antimonotonicity, chaos and multiple attractors in a novel autonomous memristor-based jerk circuit," Nonlinear Dyn. **88**(4), 2589–2608 (2017).

[36]A. Buscarino, L. Fortuna, M. Frasca, and L. V. Gambuzza, "A gallery of chaotic oscillators based on HP memristor," Int. J. Bifurcation Chaos **23**(05), 1330015 (2013).

[37]F. Y. Yang, J. L. Leng, and Q. D. Li, "The 4-dimensional hyperchaotic memristive circuit based on Chuas circuit," Acta Phys. Sin. **63**(8), 080502 (2014).

[38]B. Zhang and F. Deng, "Double-compound synchronization of six memristor-based Lorenz systems," Nonlinear Dyn. **77**(4), 1519–1530 (2014).

[39]W. Wang, Y. Zeng, and R. Sun, "Research on a six-order chaotic circuit with three memristors," Acta Phys. Sin. **66**(4), 040502 (2017).

[40]J. Zhang and X. Liao, "Synchronization and chaos in coupled memristor-based Fitzhugh-Nagumo circuits with memristor synapse," AEU-Int. J. Electron. Commun. **75**, 82–90 (2017).

[41]C. K. Volos, I. M. Kyprianidis, I. N. Stouboulos, E. Tlelo-Cuautle, and S. Vaidyanathan, "Memristor: A new concept in synchronization of coupled neuromorphic circuits," J. Eng. Sci. Technol. Rev. **8**(2), 157–173 (2015); available at https://scholar.google.com.au/scholar?cluster=14910643030463292795&hl=zh-CN&as_sdt=2005&sciodt=0,5.

[42]S. Yang, C. Li, and T. Huang, "Synchronization of coupled memristive chaotic circuits via state-dependent impulsive control," Nonlinear Dyn. **88**(1), 115–129 (2017).

[43]L. Ni, H. Huang, and H. Yu, "A memristor network with coupled oscillator and crossbar towards L2-norm based machine learning," in *IEEE/ACM International Symposium on Nanoscale Architectures (NANOARCH)* (IEEE, 2016), pp. 179–184.

[44]M. Itoh and L. O. Chua, "Memristor oscillators," Int. J. Bifurcation Chaos **18**(11), 3183–3206 (2008).

[45]B. Muthuswamy and P. P. Kokate, "Memristor-based chaotic circuits," IETE Tech. Rev. **26**(6), 417–429 (2009).

[46]C. Wang, X. Liu, and H. Xia, "Multi-piecewise quadratic nonlinearity memristor and its 2n-scroll and 2n+ 1-scroll chaotic attractors system," Chaos **27**(3), 033114 (2017).

[47]H. H. Ching Iu, D. Yu, A. L. Fitch, V. Sreeram, and H. Chen, "Controlling chaos in a memristor based circuit using a twin-T notch filter," IEEE Trans. Circuits Syst. I: Reg. Pap. **58**(6), 1337–1344 (2011).

[48]I. A. Korneev and V. V. Semenov, "Andronov–Hopf bifurcation with and without parameter in a cubic memristor oscillator with a line of equilibria," Chaos **27**(8), 081104 (2017).

[49]B. Muthuswamy, "Implementing memristor based chaotic circuits," Int. J. Bifurcation Chaos **20**(05), 1335–1350 (2010).

[50]G. Si, L. Diao, and J. Zhu, "Fractional-order charge-controlled memristor: Theoretical analysis and simulation," Nonlinear Dyn. **87**(4), 2625–2634 (2017).

[51]L. Teng, H. H. Ching Iu, X. Wang, and X. Wang, "Novel chaotic behavior in the Muthuswamy–Chua system using Chebyshev polynomials," Int. J. Numer. Modell.: Electron. Netw. Devices Fields **28**(3), 275–286 (2015).

[52]S. Cang, A. Wu, Z. Wang, Z. Wang, and Z. Chen, "A general method for exploring three-dimensional chaotic attractors with complicated topological structure based on the two-dimensional local vector field around equilibriums," Nonlinear Dyn. **83**(1-2), 1069–1078 (2016).

[53]B. Bao, N. Wang, Q. Xu, H. Wu, and Y. Hu, "A simple third-order memristive band pass filter chaotic circuit," IEEE Trans. Circuits Syst. II: Express Briefs **64**(8), 977–981 (2016).

[54]S. P. Adhikari, M. P. Sah, H. Kim, and L. O. Chua, "Three fingerprints of memristor," IEEE Trans. Circuits Syst. I: Reg. Pap. **60**(11), 3008–3021 (2013).